PROTON-EXCHANGE MEMBRANE FUEL CELL STACK MODEL

PARAMETERS ESTIMATION AND MODEL VALIDATION

by

Aya Mohamad Taieb

A Thesis presented to the Faculty of the
American University of Sharjah
College of Engineering
In Partial Fulfillment
of the Requirements
for the Degree of

Master of Science in
Electrical Engineering

Sharjah, United Arab Emirates

April 2019

Approval Signatures

We, the undersigned, approve the Master's Thesis of Aya Mohamad Taieb

Thesis Title: Proton-Exchange Membrane Fuel Cell Stack Model Parameters Estimation and Model Validation

Signature	**Date of Signature** (dd/mm/yyyy)
_____	_____
Dr. Shayok Mukhopadhyay Assistant Professor, Department of Electrical Engineering Thesis Advisor	
_____	_____
Dr. Amani Al-Othman Assistant Professor, Department of Chemical Engineering Thesis Co-Advisor	
_____	_____
Dr. Mostafa Shaaban Assistant Professor, Department of Electrical Engineering Thesis Committee Member	
_____	_____
Dr. Mehmet Orhan Associate Professor, Department of Mechanical Engineering Thesis Committee Member	
_____	_____
Dr. Nasser Qaddoumi Head, Department of Electrical Engineering	
_____	_____
Dr. Lotfi Romdhane Associate Dean for Graduate Affairs and Research College of Engineering	
_____	_____
Dr. Naif Darwish Acting Dean, College of Engineering	
_____	_____
Dr. Mohamed El-Tarhuni Vice Provost for Graduate Studies	

Acknowledgment

I would first like to thank my thesis advisors Dr. Shayok Mukhopadhyay and Dr. Amani Al-Othman for their valuable guidance and support to complete this thesis. I am deeply beholden for their great assistance, worthy discussion, and suggestions.

My thanks also go to the College of Engineering at the American University of Sharjah for supporting my study and thesis work with the graduate assistantship that made it possible for me to complete the master's degree. Also, I would like to thank Dr. Di Zhang for his support and encouragement to study for my M.Sc. degree.

A special thanks to my colleagues Ali Al-Tameemi and Usman Butt who supported and assisted me in the experimental and simulation work throughout my thesis journey.

Finally, I must express my very profound gratitude to my parents, brother, sister, and friends for providing me with unfailing support and continuous encouragement throughout my years of study, and through the process of researching and writing this thesis. This accomplishment would not have been possible without them.

Dedication

To my family…

Abstract

A proton-exchange membrane fuel cell (PEMFC) is a promising, clean, and efficient power device that converts the chemical energy stored in a fuel into electricity directly. Hydrogen is supplied from an external tank and it is oxidized at the anode of the fuel cell, this activity releases electrons, which are made to flow through an external circuit. Oxygen is supplied at the cathode where it is reduced by the electrons flowing in the external circuit. The growing popularity of using PEMFC stacks in stationary, portable, and transportation applications is driving researchers to develop dynamic models to accurately capture the electrical characteristics and runtime performance. These characteristics are critical when integrating a fuel cell stack with power conditioning units (PCUs), and power electronics onboard fuel cell powered systems. Conventional PEMFC models may be complex and substantial effort is required to estimate parameters of such models. This work establishes a simple equivalent electrical circuit model of a PEMFC stack that captures the voltage-current (V-I) runtime characteristics under different load, and under different hydrogen flow rate conditions. It proposes a well-known equivalent circuit model of a battery, to be modified and used, as a model for a PEMFC stack. The existing adaptive parameters estimation (APE) technique is used to estimate the proposed PEMFC stack's model parameters. Also, the concept of the state of charge (SoC) of a battery is thought as analogous to the amount of hydrogen available in a PEMFC stack's supply tank. In this work, an existing battery model is modified to model the electrical performance of a 200-W PEMFC stack. All the model parameters are estimated using the APE technique that is known to require few experiments. The model is validated experimentally under different load conditions for the 200-W PEMFC stack. In addition, the model is validated with a different fuel cell stack of a smaller size, i.e. a 30-W PEMFC stack. All results show reasonably accurate terminal voltage estimation with error in the order of millivolts, and 95.84% of the all samples of estimated terminal voltage have between ± 0.1% error compared to the actual terminal voltage.

Keywords: ***Proton-Exchange Membrane Fuel Cell Stack; Dynamic Model; Adaptive Parameters Estimation; Universal Adaptive Stabilization***

Table of Contents

List of Figures

List of Tables

List of Abbreviations

ADC	Analog to Digital Converter
APE	Adaptive Parameters Estimation
BJTs	Bipolar Junction Transistor
CM	Chen and Mora
CO	Carbon monoxide
DAC	Digital to Analog Converter
DMFC	Direct Methanol Fuel Cell
LFL	Low Flammability Level
ODEs	Ordinary Differential Equations
PCUs	Power Conditioning Units
PDEs	Partial Differential Equations
PEMFC	Proton Exchange Membrane Fuel Cell
PWM	Pulse Width Modulation
SoC	State of Charge
UAS	Universal Adaptive Stabilization
V-I	Voltage-Current

Chapter 1. Introduction

1.1. Overview

Fuel cells are gaining popularity as a promising alternative to energy storage devices like batteries and conventional power generation sources. The chemical energy of the fuel is converted directly to electricity, avoiding producing heat and mechanical work as intermediate steps, thus generating power with relatively high efficiency compared to generators with moving parts, and with minimized emission of pollutants. Both, a fuel cell, and a battery operate by utilizing electrochemical reactions between a reductant and an oxidant to generate electricity. However, a battery must be recharged or replaced when it dies whereas, a fuel cell supplies power as long as the required fuel and oxidant are provided continuously. A fuel cell usually has higher energy density compared to a battery, however, it may use a lot of space to accommodate all the necessary circuitry, fuel tanks, fuel injection, and control equipment [1], [2]. Proton-exchange membrane fuel cell (PEMFC), the focus of this thesis, operates at relatively low temperature (up to 80 ºC) allowing quick start-up with easy and safe operation modes, as well as, an all solid structure. Such a fuel cell uses a polymer membrane known as Nafion (perfluorinated sulfonic acid), that has excellent proton conductivity, and resistance to gas crossover. The electrodes are made of the precious metal platinum supported on carbon. Therefore, only pure hydrogen is used as fuel because the platinum catalyst is easily poisoned by carbon monoxide (CO), sulfur species, and halogens. Oxygen in the air is used as the oxidant [1], [3]. Electrolysis of water provides a clean source of pure hydrogen generation [4]. In most common use however, a single fuel cell provides very low voltage and current output (around 1.2 V for a hydrogen fuel cell), so many fuel cells are usually stacked together and connected in series to boost the voltage rating, and the current rating can be boosted by increasing the fuel cell's surface area.

PEMFC stacks are used in stationary power plants, transportation, aerospace, and portable applications because they provide reliable power at steady-state. However, a PEMFC stack responds slowly to electrical load transients due to its slow internal electrochemical response. Also, supplying fuel at a constant rate is usually difficult because of the fuel pressure drop through the stack, and the limited space or volume for storing hydrogen [2], [5], [6]. To accurately model the effects of change in fuel supply,

changing load or changing internal conditions, an accurate dynamic model is needed to predict the voltage-current (V-I) behavior over time, unlike steady-state models presented in [7]–[12]. This time-dependent model must capture the performance under different situations, such as electric load variations, hydrogen flow rate or pressure variations, electrical faults on the terminals, and motor starting or acceleration in transportation applications (e.g., electric vehicle) [5]. Although there is literature existing, which provides very detailed dynamic models for fuel cells, such models are incredibly complex, for quick integration and simulation of a power system's performance when using fuel cell stacks. Therefore, this thesis proposes a simplified model of a PEMFC stack which provides sufficiently accurate V-I characteristics. Such a model aims at facilitating control design in control loops involving PEMFC stacks, where the interest is modeling, and subsequent prediction of the electrical characteristics of the PEMFC stack.

1.2. Literature Review

Electrochemical, mathematical, and equivalent electrical circuit-based models are the three main types of PEMFC models available in the literature.

Electrochemical models are used to describe the physical and chemical characteristics of a fuel cell, including mass transport, electrochemical kinetics, thermal gradients, etc. A dynamic electrochemical model for a PEMFC stack is presented in [13]. This model evaluates the electrical performance in the commonly encountered situations like load changes and power failures in electrical power generation systems. The simulation results from the model give a good agreement with the experimental data with less than 3% absolute error. An impedance model of a PEMFC stack is developed in [14] which studies the effects of inverter ripple current when a fuel cell stack is connected to power conditioning units (PCUs). Another physics-based model is reported in [15] which studies the impedance due to hydrogen crossover that affects the open-circuit voltage of a PEMFC. The hydrogen crossover is defined as the hydrogen gas diffusion from the anode to the cathode, due to the difference in concentration. This causes membrane degradation and a voltage drop. This voltage drop is maximum at open-circuit conditions. Empirical equations are developed in [16] to describe the voltage-time behavior of a PEMFC stack at a constant discharge current. The rapid fall of voltage is analyzed in different situations such as high temperature,

and with high discharge currents. These empirical equations are useful for forecasting the stacks long-term performance. Such models [13]–[16], require design parameters, which are difficult to obtain. Usually they are complex partial differential equations (PDEs), which are abstract and time intensive to solve, and may not be suitable for modeling the electrical performance i.e. when a fuel cell interacts with PCU.

Mathematical models [17]–[23], are described by empirical or semi-empirical relations that may be complex and may impose a heavy computational burden. In [18], a kinetic model is presented to investigate the platinum dissolution in a PEMFC that affects the potential and the catalyst stability. Another mathematical model in [19], is developed to model the dynamic performance that is based on physical laws. Linear and nonlinear analysis are performed in [19]. The results indicate that the linear model has errors in the modeling process. Thus, the nonlinearities must be considered to give a better prediction of the dynamic behaviors of a fuel cell stack. The control-oriented model that is represented by seventh order nonlinear of ordinary differential equations (ODEs), is used to study the steady-state and dynamical behavior of a PEMFC stack in [20]. Another control-oriented model is developed in [21] to study the thermal dynamics of a PEMFC that uses water cooling. This thermal model methodology is accurate with less than 0.14% maximum error. Optimization of PEMFC operating conditions of pressure, cathode stoichiometry, temperature, and reactants relative humidity is described by a one dimensional analytical model in [23]. The model is validated by experimental work that shows a good agreement between experimental and modeling results with a maximum error below than 3%.

On the other hand, equivalent electrical circuit models are attractive because they can provide runtime V-I dynamics under different loads and conditions, easy to implement, and less computationally intensive compared to the above types of models. A PSPICE-based simple circuit model of a PEMFC as shown in Figure 1.1 [24], is used to obtain the static and dynamic characteristics to design and analyze fuel cell power systems. A diode and a pair of bipolar junction transistors (BJTs) are used to describe the static behavior, while a capacitor and an inductor are used to represent the dynamic conditions. The activation and ohmic losses are modeled by a diode. The two BJTs model the mass transport losses. Therefore, this model includes important

phenomena that occur in the PEMFC such as the activation, mass transport, and ohmic polarizations.

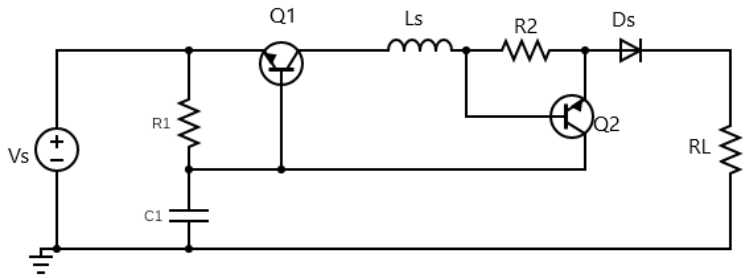

Figure 1.1: Electronic circuit model of a PEMFC.

Another dynamic model presented in [5], uses electrical circuits and has been implemented in MATLAB/SIMULINK and PSPICE environments to simulate the steady-state and dynamic conditions. The equivalent electrical circuit that model the double-layer charging effect is shown in Figure 1.2. Also, the equivalent electrical circuit that describes the thermodynamic behavior is shown in Figure 1.3.

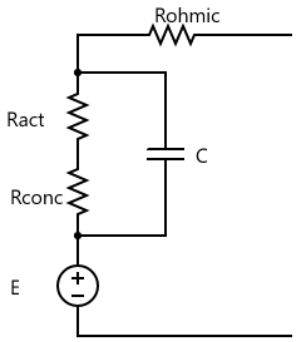

Figure 1.2: Double-layer charging effect of a PEMFC modeled using an equivalent electrical circuit.

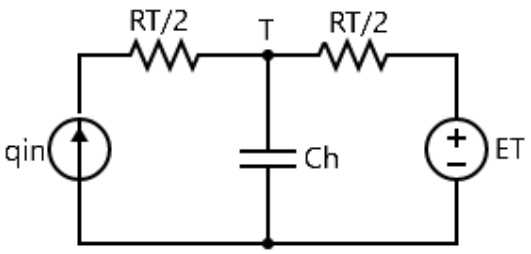

Figure 1.3: Thermodynamic model of a PEMFC using an equivalent electrical circuit.

The paper in [25], presents a model, and corresponding fault diagnosis techniques on a PEMFC using an equivalent electrical circuit. This model combines thermodynamics, fluid dynamics, electrochemistry, and electrical performance. And the diagnosis methodology is introduced to identify the parameters of the equivalent circuit model.

Other dynamic models are used to detect the performance of fuel cells in hybrid energy systems [26]–[30]. For example, dynamic modeling and simulation of a hybrid system consisting of a PEMFC stack, wind turbine, ultracapacitors, an electrolyzer, and power converters are done in [26]. An equivalent electrical circuit is used to model the PEMFC electrical performance using parametric model. Similar dynamic model and simulation are conducted in [27] to predict the electrical performance of solar photovoltaics hybrid battery and fuel cell stack system.

Nonetheless, most of these equivalent electrical circuit models are based on electrochemical equations and laws (such as Nernst and Tafel equations, Fick's and Faraday's laws) that are detailed and include many parameters whose values are usually assumed. Therefore, parameters estimation methods are needed. For example, the work in [31] deals with parameter identification and diagnostics of a PEMFC. Also, the work in [32] presents a backtracking search algorithm with Burger's chaotic map for estimating the parameters of a PEMFC electrochemical model. In addition, none of the previous models discuss the voltage drop occurring in a PEMFC stack with time, due to the hydrogen flow rate or pressure drop from an external tank.

Accordingly, a simple and accurate dynamic model for a PEMFC stack is needed, that captures the effects of a finite amount of fuel from a tank, and dynamic load changes, on the V-I relationship. Chen and Mora (CM) established a model to predict the V-I characteristics for a direct methanol fuel cell (DMFC) by considering the methanol concentration as the SoC [2]. But the fuel used in DMFC is methanol, which is liquid, while hydrogen is gas used as fuel in a PEMFC, which necessitates another model. It is observed that a fuel cell and battery have similar V-I characteristics. A hypothesis of this work is thus that, a model similar to a battery model may be a viable option to capture runtime characteristics of a PEMFC stack. Estimating battery model parameters [33] requires substantial experimental effort, which inspired the authors in [34], to establish a universal adaptive stabilization (UAS) based approach for

battery adaptive parameters estimation (APE). Modifying the battery model used in [33], [34] and estimating parameters with the help of UAS-based APE [34] has potential to provide an accurate model for a PEMFC stack, with less experimental effort compared to existing techniques in the literature, which is the main objective of this thesis.

1.3. Thesis Objectives

Driven by the importance of developing a simple, accurate, and dynamic model capturing the V-I characteristics of a PEMFC stack, this thesis aims to modify a battery model to be suitable for a PEMFC stack. Also, demonstrating that the UAS-based methodology for estimating battery model parameters adaptively, can be used to estimate model parameters for a fuel cell stack while reducing experimental effort, is another goal of this work.

1.4. Thesis Contribution

The contribution of this thesis work is summarized as follows:

- Develop a dynamic model of a PEMFC stack using equivalent electrical circuit elements.
- Estimating the parameters of the above model using the UAS-based APE methodology.
- Validate the model experimentally and study the fuel cell stack size effect on the model parameters.

1.5. Thesis Organization

The rest of the thesis is organized as follow: Chapter 2 provides background about the polarization characteristics of a PEMFC and its similarities to battery characteristics. Also, this section explains CM battery model [33] and UAS-based methodology for APE [34]. The proposed model with the APE methodology of a PEMFC stack is discussed in Chapter 3. Also, this chapter presents the model parameters estimation and the experimental setup. Then, the results of the model validation, PEMFC stack size effect, and error statistics are presented in Chapter 4. Finally, concluding remarks, and possible avenues of future work after the completion of the thesis, are given in Chapter 5.

Chapter 2. Background

In this chapter, the principle of the PEMFC is explained along with the commonly used polarization characteristics. This will give a better understating of the fuel cell concept and operation. Also, the similarities and the differences between the fuel cell and battery is discussed. Then, the CM battery model with the UAS-based APE process is explained in detail. This model is modified to model the PEMFC stack, and the APE process is used to estimate the model parameters, as will be discussed in chapter 3.

2.1. Polarization Characteristics of PEMFC

In a PEMFC, as shown in Figure 2.1, hydrogen enters the anode where it is oxidized on platinum to produce protons and electrons. Protons diffuse through the membrane and electrons are forced to flow externally toward the cathode. Thus, generating direct electrical current. At the cathode side, oxygen from the air is supplied to the cathode to react with protons coming from the membrane and electrons producing water and heat as the by-products, as below:

$$\begin{aligned} &Anode\ Reaction: H_2 \xrightarrow{yields} 2H^+ + 2e^- \\ &Cathode\ Reaction: \frac{1}{2}O_2 + 2H^+ + 2e^- \xrightarrow{yields} H_2O \\ &Overall\ Reaction: H_2 + \frac{1}{2}O_2 \xrightarrow{yields} H_2O + Heat \end{aligned} \tag{1}$$

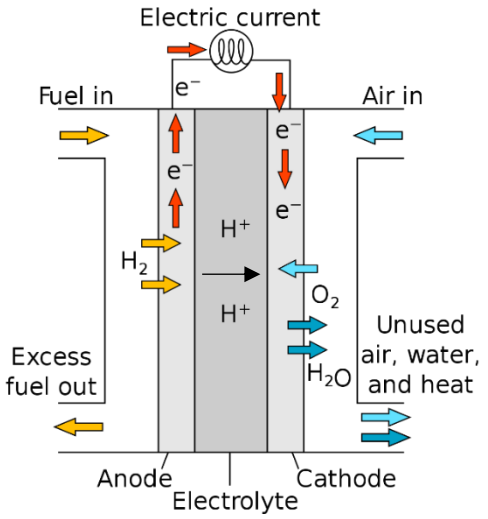

Figure 2.1: Schematic diagram of a PEMFC [35].

The polarization curve (V-I) of a typical PEMFC is shown in Figure 2.2, indicating the theoretical voltage as 1.2 V (for reaction 1) considering no internal losses. However, there are three major phenomena occurring inside the fuel cell, which cause a voltage drop as more current is drawn. These are activation, concentration, and ohmic polarizations. Fuel crossover is also considered as a major problem, which is caused by the fuel passing through the membrane, causing combustion. But, the effect of this loss is small compared to other losses at low temperatures [3]. The major polarizations are explained in detail as follows:

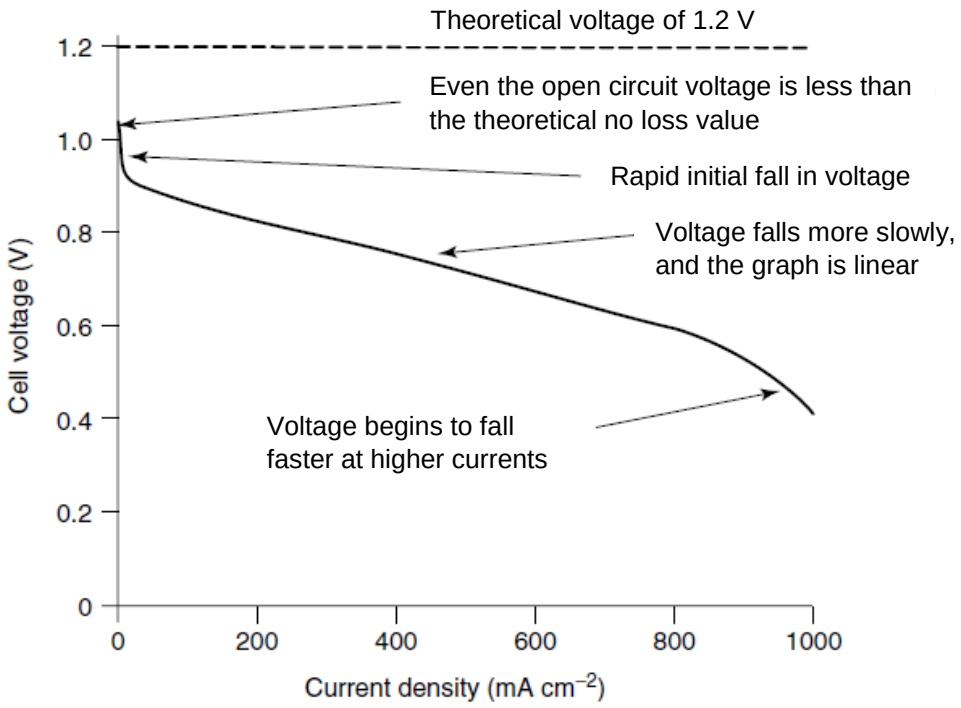

Figure 2.2: V-I characteristics curve of a PEMFC operating at 70 ºC [3].

2.1.1. Open-circuit voltage. The theoretical voltage $E_{theoretical}$ of a PEMFC, indicated by the flat line shown in Figure , is calculated from equation (2),

$$E_{theoretical} = -\frac{\Delta G}{nF} \quad (2)$$

where ΔG is the Gibbs free energy of the water formation reaction, which is equal to -226522 J/mol at 70 ºC [36], n represents the number of electrons transferred from 1 mole of hydrogen (equal to 2 electrons), and F is Faraday's constant equal to 96458 C/mol. The open-circuit voltage of a PEMFC is less than 1.2 V, due to the change of Gibbs free energy with the change of reactants and products pressure and activation

energy [3]. Nernst equation is used to obtain the actual open-circuit voltage E considering that change, defined as:

$$E = E_{theoretical} + \frac{RT}{nF} ln\left(\frac{P_{H_2} P_{O_2}^{0.5}}{P_{H_2O}}\right) \quad (3)$$

where R is the universal gas constant equal to 8.314 J/K mol, T is the operating cell temperature in degrees Kelvin, P_{H_2}, P_{O_2}, and P_{H_2O} are the partial pressure (the pressure exerted by each gas in a mixture) of hydrogen, oxygen, and water in atm, respectively. The second term in (3) must be negative for E to become less than $E_{theoretical}$ at open-circuit mode. That means the magnitude of the numerator term within the natural log operator, is less compared to the denominator.

2.1.2. Activation polarization. Part of the generated voltage is lost to overcome the activation energy and drive the chemical reaction that transfers the electrons between the electrodes. This speed or kinetics of reactions at the surface of electrodes is dominant at low current densities. The activation voltage drop V_{act} is non-linear and can be obtained from the Tafel equation, described in equation (4),

$$V_{act} = \frac{RT}{n\alpha F} \ln\left(\frac{I}{I_o}\right) \quad (4)$$

where α is the charge transfer coefficient, I is the current density in mA/cm^2, and I_o is the exchange current density at which the overvoltage begins to move from zero. Tafel equation only holds true when $I > I_o$ [3].

2.1.3. Concentration polarization. This kind of polarization is associated with the concentrations or pressure reduction of reactants (fuel and oxidant) at the surface of electrodes as they are consumed, because of a current being drawn from the fuel cell. At high current densities, the fuel cell fails in transporting sufficient reactants to the surface of electrodes, causing a high voltage to drop, due to the accumulation of water produced in the hydrogen fuel cell for example [3]. The voltage drop due to concentration polarization V_{conc} is given in equation (5),

$$V_{conc} = \frac{RT}{nF} ln\left(1 - \frac{I}{I_L}\right) \quad (5)$$

where I_L is the limiting or the maximum current density that a certain fuel cell can produce.

2.1.4. Ohmic polarization. The linear voltage drop V_{Ohm} due to the resistance (R_{ohm} in kΩ.cm^2) to ion flow through the electrodes, membrane, and other electrical interconnections can be obtained directly from Ohm's law as:

$$V_{Ohm} = IR_{ohm} \tag{6}$$

Therefore, the terminal voltage V of fuel cells considering all the voltage losses can be obtained from equation (7), where N is the number of cells connected in series in a single stack. More simply, all the losses can be obtained from equation (8) [3],

$$V = N[E - V_{act} - V_{conc} - V_{Ohm}] \tag{7}$$

$$V = N[E - IR_{ohm} - Aln(I) - mexp(nI)] \tag{8}$$

where A is the slope of Tafel equation described in (4), m and n are the constants for the mass-transfer empirical equation, that has lately become more favored than equation (5) because it is simple and gives a very good fit to actual results [37], [38].

2.2. Battery and Fuel Cell Characteristics

Batteries and fuel cells are electrochemical devices that convert stored chemical energy to electricity by a couple of redox reactions. Thus, they produce a DC current and share the same polarization characteristics, as discussed in the previous section. In a battery, the chemicals are stored inside it, and the energy capacity is represented by its state of charge SoC. Similarly, a fuel cell has a finite fuel capacity, usually from fuel stored in an external tank. The amount of hydrogen supplied to a PEMFC can be thought of as analogous to SoC for a battery. This "SoC" for a fuel cell, can be obtained from the hydrogen flow rate or pressure measurements. Due to the similarities between a battery and a fuel cell, battery dynamic models can be adapted to model PEMFC dynamics.

2.2.1. CM battery model. The equivalent electrical circuit model of Li-ion battery [33], shown in Figure 2.3, captures all the essential dynamic behavior of a battery including open-circuit voltage, terminal voltage, and parameters variation with the change in SoC. The model has been verified by extensive experimentation achieving less than 0.4% runtime error and 30-mV maximum voltage estimation error. Hence, the

model predicts the V-I runtime performance of a battery accurately, and it is versatile [33], motivating us to establish a similar model for a PEMFC stack. The left half of the equivalent circuit in Figure 2.3 models the SoC dynamics, while the right half represents the output voltage dynamics. Equations (9)-(12) show the state-space representation of the CM model [34].

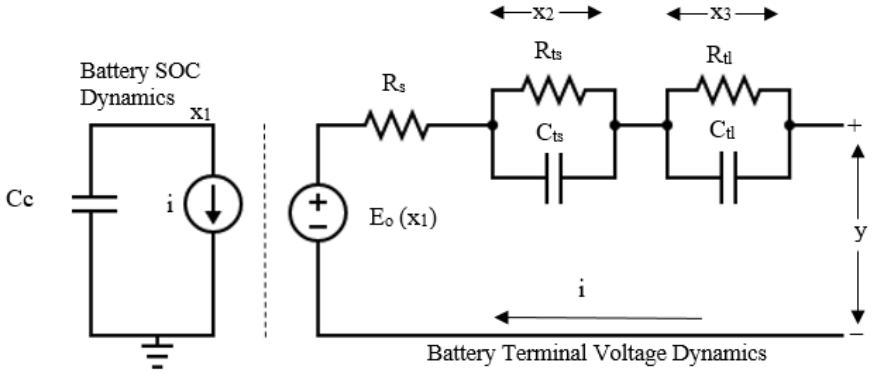

Figure 2.3: The CM equivalent electrical circuit model of a Li-ion battery.

$$\dot{x}_1(t) = -\frac{1}{C_c} i(t), C_c = 3600 C f_1 f_2 f_3 \tag{9}$$

$$\dot{x}_2(t) = -\frac{x_2(t)}{R_{ts}(x_1) C_{ts}(x_1)} + \frac{i(t)}{C_{ts}(x_1)} \tag{10}$$

$$\dot{x}_3(t) = -\frac{x_3(t)}{R_{tl}(x_1) C_{tl}(x_1)} + \frac{i(t)}{C_{tl}(x_1)} \tag{11}$$

$$y(t) = E_o(x_1) - x_2(t) - x_3(t) - i(t) R_s(x_1) \tag{12}$$

In equation (9), x_1 is the SoC $\in [0,1]$, C is the capacity of the battery in ampere-hours (Ah), and the factors $f_1, f_2, f_3 \in [0,1]$ account for the effects of temperature, number of charge-discharge cycles, and self-discharge, respectively. By default and for simplicity $f_1 = f_2 = f_3 = 1$. In equations (10) and (11), x_2 and x_3 are the voltages across $R_{ts}||C_{ts}$ and $R_{tl}||C_{tl}$ (non-negative real numbers), respectively. The parallel combination $R_{ts}||C_{ts}$ and $R_{tl}||C_{tl}$ model the short-term, and long-term terminal voltage dynamics, respectively. The battery terminal voltage $y(t)$ in equation (12), depends on open-circuit voltage E_o, the voltage drops x_2, x_3, discharge current i, and battery series resistance R_s. The circuit elements E_o, R_{ts}, R_{tl}, C_{ts}, C_{tl}, and R_s are obtained as below:

$$E_o(x_1) = -a_1 e^{-a_2 x_1} + a_3 + a_4 x_1 - a_5 x_1^2 + a_6 x_1^3 \quad (13)$$

$$R_{ts}(x_1) = a_7 e^{-a_8 x_1} + a_9 \quad (14)$$

$$R_{tl}(x_1) = a_{10} e^{-a_{11} x_1} + a_{12} \quad (15)$$

$$C_{ts}(x_1) = -a_{13} e^{-a_{14} x_1} + a_{15} \quad (16)$$

$$C_{tl}(x_1) = -a_{16} e^{-a_{17} x_1} + a_{18} \quad (17)$$

$$R_s(x_1) = a_{19} e^{-a_{20} x_1} + a_{21} \quad (18)$$

The parameters $a_n > 0$ for $n = \{1,2,3 \ldots,21\}$. In this model, extracting all the parameters requires considerable experimental effort. Consequently, a UAS-based technique is used to determine these parameters accurately, and also reducing the experimental effort [34].

2.3. UAS-Based Approach for APE

The UAS-based approach, in [34], helps in reducing the number of experiments needed to estimate CM battery model parameters. This is achieved by tuning the values of the parameters until the error, between the estimated output voltage and the real measured terminal voltage, is negligibly small. A Nussbaum function is used as a switching function for APE and is discussed in section **2.3.1**. Then, the problem setup with the steps of the APE technique is provided in section **2.3.2**. The below details are presented directly from [34].

2.3.1. Mittag-Leffler function as a Nussbaum function. Nussbaum functions are a class of switching functions used for designing UAS [39]–[41]. A piecewise right continuous and locally Lipschitz function $N(\cdot) : [k', \infty) \rightarrow \mathbb{R}$, where $k' \in \mathbb{R}$, is a Nussbaum function if it satisfies (20) for some $k_o \in (k', \infty)$. A Mittag-Leffler function, described in equation (19), is used as Nussbaum function for CM model parameters estimation, because it has a very fast growth rate and hence provides high speed for the error (between estimated and actual output voltage), to convergence to zero,

$$E_\alpha(z) = \sum_{k=0}^{\infty} \frac{z^k}{\Gamma(k\alpha + 1)} \tag{19}$$

$$\begin{cases} sup_{k>k_o} \dfrac{1}{k - k_o} \displaystyle\int_{k_o}^{k} N(\tau)d\tau \;\; = +\infty \\ inf_{k>k_o} \dfrac{1}{k - k_o} \displaystyle\int_{k_o}^{k} N(\tau)d\tau \;\; = -\infty \end{cases} \tag{20}$$

where $\Gamma(z+1) = z\Gamma(z), z > 0$ is the standard Gamma function, $\alpha \in (2,3)$ and $\lambda > 0$, for (19) to be considered as a Nussbaum function [39]. The details of implementing equation (19) in MATLAB is available in [42].

2.3.2. Problem setup and steps. The APE methodology in [34] is divided into three main steps, as shown in Figure 2.4, based on the following observer model, when the battery is discharging:

$$\dot{\hat{x}}_1(t) = -\frac{1}{C_c} i(t), C_c = 3600 C f_1 f_2 f_3, \hat{x}_1 \epsilon\, [0,1] \tag{21}$$

$$\dot{\hat{x}}_2(t) = -\frac{\hat{x}_2(t)}{\hat{R}_{ts}(\hat{x}_1)\hat{C}_{ts}(\hat{x}_1)} + u(t), \hat{x}_2 \geq 0 \tag{22}$$

$$\dot{\hat{x}}_3(t) = -\frac{\hat{x}_3(t)}{\hat{R}_{tl}(\hat{x}_1)\hat{C}_{tl}(\hat{x}_1)} + u(t), \hat{x}_3 \geq 0 \tag{23}$$

$$\hat{y}(t) = E_o(\hat{x}_1) - \hat{x}_2 - \hat{x}_3 \tag{24}$$

$$\hat{E}_o(\hat{x}_1) = -\hat{a}_1 e^{-\hat{a}_2 \hat{x}_1} + \hat{a}_3 + \hat{a}_4 \hat{x}_1 - \hat{a}_5 \hat{x}_1^2 + -\hat{a}_6 \hat{x}_1^3 \tag{25}$$

$$\hat{R}_{ts}(\hat{x}_1) = \hat{a}_7 e^{-\hat{a}_8 \hat{x}_1} + \hat{a}_9 \tag{26}$$

$$\hat{R}_{tl}(\hat{x}_1) = \hat{a}_{10} e^{-\hat{a}_{11} \hat{x}_1} + \hat{a}_{12} \tag{27}$$

$$\hat{C}_{ts}(\hat{x}_1) = -\hat{a}_{13} e^{-\hat{a}_{14} \hat{x}_1} + \hat{a}_{15} \tag{28}$$

$$\hat{C}_{tl}(\hat{x}_1) = -\hat{a}_{16} e^{-\hat{a}_{17} \hat{x}_1} + \hat{a}_{18} \tag{29}$$

$$\hat{R}_s(\hat{x}_1) = \hat{a}_{19} e^{-\hat{a}_{20} \hat{x}_1} + \hat{a}_{21} \tag{30}$$

The quantity $\hat{x}_1$ is considered as an SoC estimate at a time step similar to x_1. It is estimated using the battery capacity C and discharges current i. The estimated voltage drops $\hat{x}_2$ and $\hat{x}_3$ can only be positive during battery discharge. In the observer model (equations (21)-(24)), the original CM model (equations (9)-(12)) is slightly modified to prove that the error between the actual and estimated output voltage converges to zero with time. This is described in the second step of the APE process.

The first step is obtaining the open-circuit voltage $\hat{E}_o(\hat{x}_1)$ curve of a given Li-ion battery from the voltage relaxation test mentioned in [43]. This test requires discharging a given battery for a small period of time followed by a roughly similar or longer period of rest. The discharging-resting process is repeated until the battery is completely discharged (SoC must be slightly less than 10%, and not reduced all the way to zero, to avoid battery damage). At each rest time instant, the battery terminal voltages are recorded, accounting for the estimated open-circuit voltages $\hat{E}_o(\hat{x}_1(t))$. While, the values of discharge current when the battery is supplying the load, are recorded to be used in equation (21), to get $\dot{\hat{x}}_1(t)$. The parameters $\hat{a}_1, \dots, \hat{a}_6$ can be easily obtained by fitting equation (25) to the above terminal voltage measurements and SoC, using a software package such as the MATLAB 'Curve fitting toolbox'.

The second step is performing the APE technique using the following UAS-based observer:

$$e(t) = y(t) - \hat{y}(t) \tag{31}$$

$$\dot{k}(t) = e^2(t), k(t_o) = k_o \tag{32}$$

$$N\big(k(t)\big) = E_\alpha(\lambda k(t)^\alpha), \lambda > 0\ \alpha\ \in (2,3) \tag{33}$$

$$u(t) = -N(k(t))e(t) \tag{34}$$

where e is the error signal between the real battery terminal voltage (y) and the estimated terminal voltage ($\hat{y}$). Then, equation (35) is used to obtain the parameters $\hat{a}_7, \dots, \hat{a}_{18}$, thus providing $\hat{R}_{ts}$, $\hat{R}_{tl}$, $\hat{C}_{ts}$, and $\hat{C}_{tl}$ via (26)-(29) at each time step. In (35), a_{nu} and $a_{nl} \in \mathbb{R} \geq 0$ represent the steady-state upper and lower bounds of $\hat{a}_n$, respectively. Constants λ_{x_n} and $\lambda_{y_n} \in \mathbb{R} \geq 0$ are weights accounting for the user's confidence in his/her estimates of upper and lower bounds a_{nu}, a_{nl}, respectively.

$$\begin{gathered}\dot{\hat{a}}_n(t) = e^2(t) + \lambda_{x_n}\big(a_{nu} - \hat{a}_n(t)\big) + \lambda_{y_n}\big(a_{nl} - \hat{a}_n(t)\big), \\ \hat{a}_n > 0\ for\ n\ \in \{7,8,\dots.,18\}.\end{gathered} \tag{35}$$

The procedure of the APE is represented in pseudocode form, in **Algorithm 1**, which lists its physical requirements, inputs, initial conditions, and outputs. It is performed at a very small magnitude of discharge current, $i(t) \neq 0, 0 < i(t) < \epsilon$. The values of the equivalent electrical circuit elements ($\hat{R}_{ts}$, $\hat{R}_{tl}$, $\hat{C}_{ts}$, and $\hat{C}_{tl}$) are calculated at every time step using equations (26)-(29), capturing the effect and dependency of the change in SoC. **Algorithm 1** can run for a specified time by specifying the initial time instant $t_{initial}$, a time step size t_{step}, and a termination time t_{final}. It has been found that the suitable values of t_{step} are ranging from 0.01 to 0.1 second, and t_{final} is a value larger than the time required to completely drain the battery whose parameters are being estimated while supplying the average load current. During each time step, y, i, are measured, and $\hat{y}$ is estimated. Then, e is obtained and used to compute the adaptive control signal u which tries to drive the error to zero. Also, the model parameters $\hat{a}_n$ for $n \in \{7,8, \dots ,18\}$ are computed. If e is within a pre-set small bound, then **Algorithm 1** returns certain values for $\hat{a}_n$ and continues executing the loop, else a null value is returned. The conditions presented in **Lemma 1**, are required to be satisfied for obtaining valid parameters estimates. At the end of **Algorithm 1**, the last non-null $\hat{a}_n$ values represent the estimated values of parameters $[\hat{a}_7, \dots, \hat{a}_{18}]$ used in state equations of the CM model of Li-ion battery.

Lemma 1: *Let* $n = \{13,15,16,18\}$. *Suppose* $\lambda_{x_n}, \lambda_{y_n}, a_{nu}, a_{nl}$ *are positive real numbers. Further Let* $\mathbf{1} = [1\ 1]^T, \boldsymbol{\Lambda}_n = \left[\lambda_{x_n}\ \ \lambda_{y_n}\right]^T, \boldsymbol{P}_n = [a_{nu}\ \ a_{nl}]^T$, *then the following statements hold for* $\hat{x}_1(t) \in (0,1]$

1. *If* $0 < \hat{a}_{15}(t_{initial}) < \hat{a}_{13}(t_{initial})$, $\mathbf{1}^T\boldsymbol{\Lambda}_{15} > \mathbf{1}^T\boldsymbol{\Lambda}_{13}$, $\mathbf{P}_{15}^T\,\boldsymbol{\Lambda}_{15} < \mathbf{P}_{13}^T\,\boldsymbol{\Lambda}_{13}$, *and* $\hat{a}_{14}(t) > -\frac{1}{\hat{x}_1(t)}\ln\left(\frac{\hat{a}_{15}(t)}{\hat{a}_{13}(t)}\right)$, *then* $\hat{C}_{ts}\left(\hat{x}_1(t)\right) > 0$
2. *If* $0 < \hat{a}_{18}(t_{initial}) < \hat{a}_{16}(t_{initial})$, $\mathbf{1}^T\boldsymbol{\Lambda}_{18} > \mathbf{1}^T\boldsymbol{\Lambda}_{16}$, $\mathbf{P}_{18}^T\,\boldsymbol{\Lambda}_{18} < \mathbf{P}_{16}^T\,\boldsymbol{\Lambda}_{16}$, *and* $\hat{a}_{17}(t) > -\frac{1}{\hat{x}_1(t)}\ln\left(\frac{\hat{a}_{18}(t)}{\hat{a}_{16}(t)}\right)$, *then* $\hat{C}_{tl}\left(\hat{x}_1(t)\right) > 0$

Proof: See [34] for proof.

Lemma 1 above, is required to guarantee that the capacitances $\hat{C}_{ts}\left(\hat{x}_1(t)\right)$ and $\hat{C}_{tl}\left(\hat{x}_1(t)\right)$ are positive when the UAS-based APE process is executed. The positivity of these capacitances is required to show that the APE process drives the error between the observed and the estimated battery terminal voltage to zero. As mentioned above, mathematical details are available in [34].

Algorithm 1: Adaptive Li-ion battery parameter estimation algorithm (pseudocode)

Physical requirements: A fully charged Li-ion battery, appropriate discharge and data acquisition circuitry.

Inputs: Initial time $t_{initial}$, time step t_{step}, termination time t_{final}, parameters $\hat{a}_1, \dots, \hat{a}_6$ from step 1, parameters $\hat{a}_n(t_{initial})$, a_{nu}, a_{nl}, λ_{x_n}, λ_{y_n} for $n \in \{7, \dots, 18\}$ satisfying conditions required for **Lemma 1** to hold. Small positive discharge current $i(t)$ for $t \geq t_{initial}$. Adaptive tracking error bound $\epsilon_2 > 0$ (smaller values of ϵ_2 increase accuracy), battery capacity C (Ah).

Initial conditions: $\hat{x}_1(t_{initial}) = 1$, $\hat{x}_2(t_{initial}) = \hat{x}_3(t_{initial}) = 0$, $\hat{y}(t_{initial}) = y(t_{initial})$.

Outputs: Estimated battery parameters $[\hat{a}_7, \dots, \hat{a}_{18}]$.

1: **for** $t = t_{initial} : t_{step} : t_{final}$ **do**
2: Read measured battery terminal voltage y, battery discharge current i.
3: Calculate $e = y - \hat{y}$
4: Find u as per equation (34)
5: Get estimated parameters $\hat{a}_n$ according to equation (35) for $n \in \{7, \dots, 18\}$.
6: Calculate $\hat{R}_{ts}$, $\hat{R}_{tl}$, $\hat{C}_{ts}$, C_{tl} using equation (26)-(29).
7: Compute state estimates $\hat{x}_1$, $\hat{x}_2$, $\hat{x}_3$ using equations (21)-(23).
8: Update estimated terminal voltage $\hat{y}$ using equation (24).
9: **if** $e < \epsilon_2$ and conditions for **Lemma 1** to hold are satisfied **then**
10: **Return** $[\hat{a}_7, \dots, \hat{a}_{18}]$
11: **Continue** loop execution
12: **else**
13: **Return Null**
14: **Continue** loop execution
15: **end if**
16: **end for**

In step 3, equation (36) is used to obtain $\hat{R}_s(\hat{x}_1(t))$. Then, curve fitting techniques are used to fit equation (30) to the values of $\hat{R}_s(\cdot)$ and obtain estimates of the parameters $[\hat{a}_{19}, \dots, \hat{a}_{21}]$. It is recommended to perform the voltage relaxation test in step 2 under different values of discharge current and consider the average value of the $\hat{E}_o$ for the different loads. A similar process is used for determining $\hat{R}_s$.

$$\hat{R}_s(\hat{x}_1(t)) = i(t)^{-1}\left(\hat{E}_o(\hat{x}_1(t)) - x_2^*(t) - x_3^*(t) - y(t)\right)$$
$$Where\ 0 < i(t) < \epsilon, \text{ and}$$
$$x_2^*(t) = x_2(t)|_{R_{ts}\to\hat{R}_{ts}, C_{ts}\to\hat{C}_{ts}}$$
$$x_3^*(t) = x_3(t)|_{R_{tl}\to\hat{R}_{tl}, C_{tl}\to\hat{C}_{tl}} \quad (36)$$

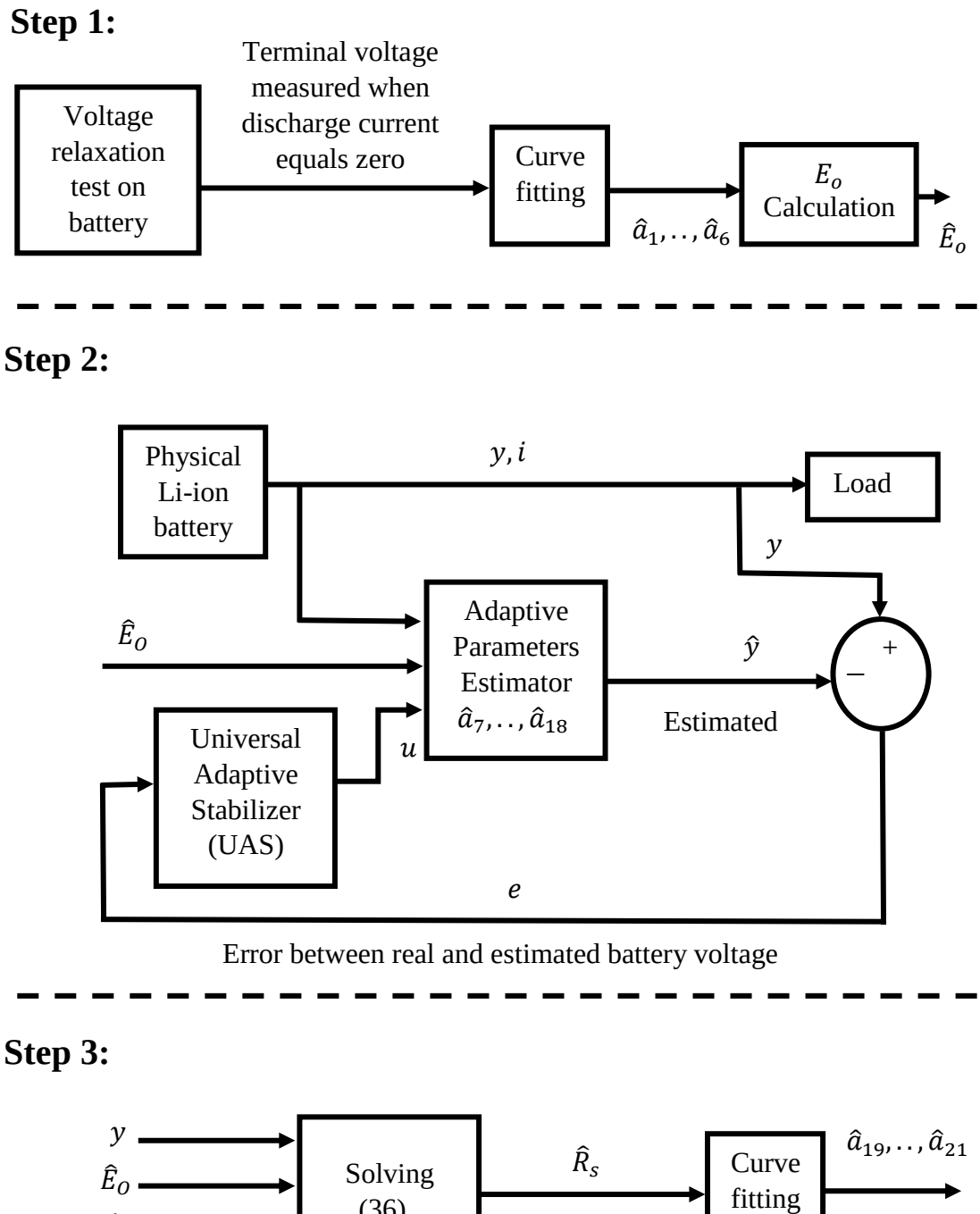

Figure 2.4: Three steps of the parameters estimation methodology for the Li-ion battery [34].

Chapter 3. PEMFC Stack Equivalent Circuit Model Parameters Estimation

In this chapter, the elements of the proposed equivalent electrical circuit model are explained. This model is a modification of the CM battery model. The experimental setup for two sizes of PEMFC stack is also shown in this chapter. This experimental setup is used to get real data to estimate the model parameters of the two PEMFC stacks (200-W and 30-W) and for model validation. In the end, the model parameters of the 200-W PEMFC stack is obtained using real data extracted from the experimental setup. The model parameters estimation is done in three main steps that are summarized in Figure 3.1.

3.1. Proposed Model

The proposed equivalent circuit model of a PEMFC stack is shown in Figure 3.2. As mentioned before, this model is based on the CM battery model [33]. Different types of fuel cell require different inlet hydrogen flow rate, hence for simplicity normalized hydrogen flow rate is considered as analogous to the SoC of a battery, for a PEMFC stack. Therefore, for our fuel cell stack, the normalized hydrogen flow rate is represented by $x_1 \in [0,1]$ and can be obtained from the hydrogen flow rate measurements experimentally. In this model, all the equivalent electrical circuit elements are functions of x_1. The open-circuit voltage of a PEMFC stack changes at different levels of input hydrogen flow rate. Thus, it is important to include a nonlinear relation between the open-circuit voltage E_o and x_1 in the model. This relation is represented by a voltage-controlled voltage source as illustrated in Figure 3.2. Equation (41) is estimated to model the open-circuit voltage as discussed in section **3.3.1**. PEMFC stack terminal voltage responds slowly to load current changes, due to the slow internal thermodynamics and electrochemical response [5]. The transient response is characterized by RC networks as follows. Two parallel combinations of RC are used to model the terminal voltage dynamics, instead of one or three, because it has the best trade-off between accuracy and simplicity. Thus, $R_{ts}||C_{ts}$ and $R_{tl}||C_{tl}$ (given in equations (42)-(45)) are used to model the short-term, and long-term, terminal voltage dynamics, respectively. These two RC parallel combinations represent the double-layer charging effect. In a PEMFC, two charged layers of opposite polarity are formed at the surface of the anode and cathode. They are known as double layers that can store energy and behave as a super-capacitor [5]. The voltage drops x_2 and x_3 across the two RC

parallel combinations are given in equations (38) and (39), respectively. The last element is the series resistance R_s which is responsible for the instantaneous voltage drop and is given in equation (46). It represents the resistance of ions flow through the membrane, electrode, and other electrical interconnection. Estimating the model parameters $[\hat{b}_1,..,\hat{b}_{33}]$ is done using the real discharge data extracted from the experimental setup (discussed in section **3.2**), and the model parameters estimation methodology (discussed in section **3.3)** as shown in Figure 3.1. In the first step, a new relation is obtained for the open-circuit voltage with estimating its parameters $[\hat{b}_1,..,\hat{b}_{18}]$. In the second step, the parameters of the two RC parallel combinations $[\hat{b}_{19},..,\hat{b}_{30}]$ are estimated using the APE technique. A new relation for the series resistance is obtained with estimating its parameters $[\hat{b}_{31},..,\hat{b}_{33}]$ in step three. The experimental setup and the model parameters estimation are discussed in detail in the following section.

$$x_1\text{: Normalized Hydrogen Flow Rate} \in [0,1] \tag{37}$$

$$\dot{x}_2(t) = -\frac{x_2(t)}{R_{ts}(x_1)C_{ts}(x_1)} + \frac{i(t)}{C_{ts}(x_1)} \tag{38}$$

$$\dot{x}_3(t) = -\frac{x_3(t)}{R_{tl}(x_1)C_{tl}(x_1)} + \frac{i(t)}{C_{tl}(x_1)} \tag{39}$$

$$y(t) = E_o(x_1) - x_2(t) - x_3(t) - i(t)R_s(x_1) \tag{40}$$

$$\begin{aligned} E_o(x_1) = {} & b_1 e^{\left(-\frac{x_1-b_2}{b_3}\right)^2} + b_4 e^{\left(-\frac{x_1-b_5}{b_6}\right)^2} + b_7 e^{\left(-\frac{x_1-b_8}{b_9}\right)^2} + b_{10} e^{\left(-\frac{x_1-b_{11}}{b_{12}}\right)^2} \\ & + b_{13} e^{\left(-\frac{x_1-b_{14}}{b_{15}}\right)^2} + b_{16} e^{\left(-\frac{x_1-b_{17}}{b_{18}}\right)^2} \end{aligned} \tag{41}$$

$$R_{ts}(x_1) = b_{19} e^{-b_{20}x_1} + b_{21} \tag{42}$$

$$R_{tl}(x_1) = b_{22} e^{-b_{23}x_1} + b_{24} \tag{43}$$

$$C_{ts}(x_1) = -b_{25} e^{-b_{26}x_1} + b_{27} \tag{44}$$

$$C_{tl}(x_1) = -b_{28}\, e^{-b_{29}\, x_1} + b_{30} \tag{45}$$

$$R_s(x_1) = -b_{31} x_1^{b_{32}} + b_{33} \tag{46}$$

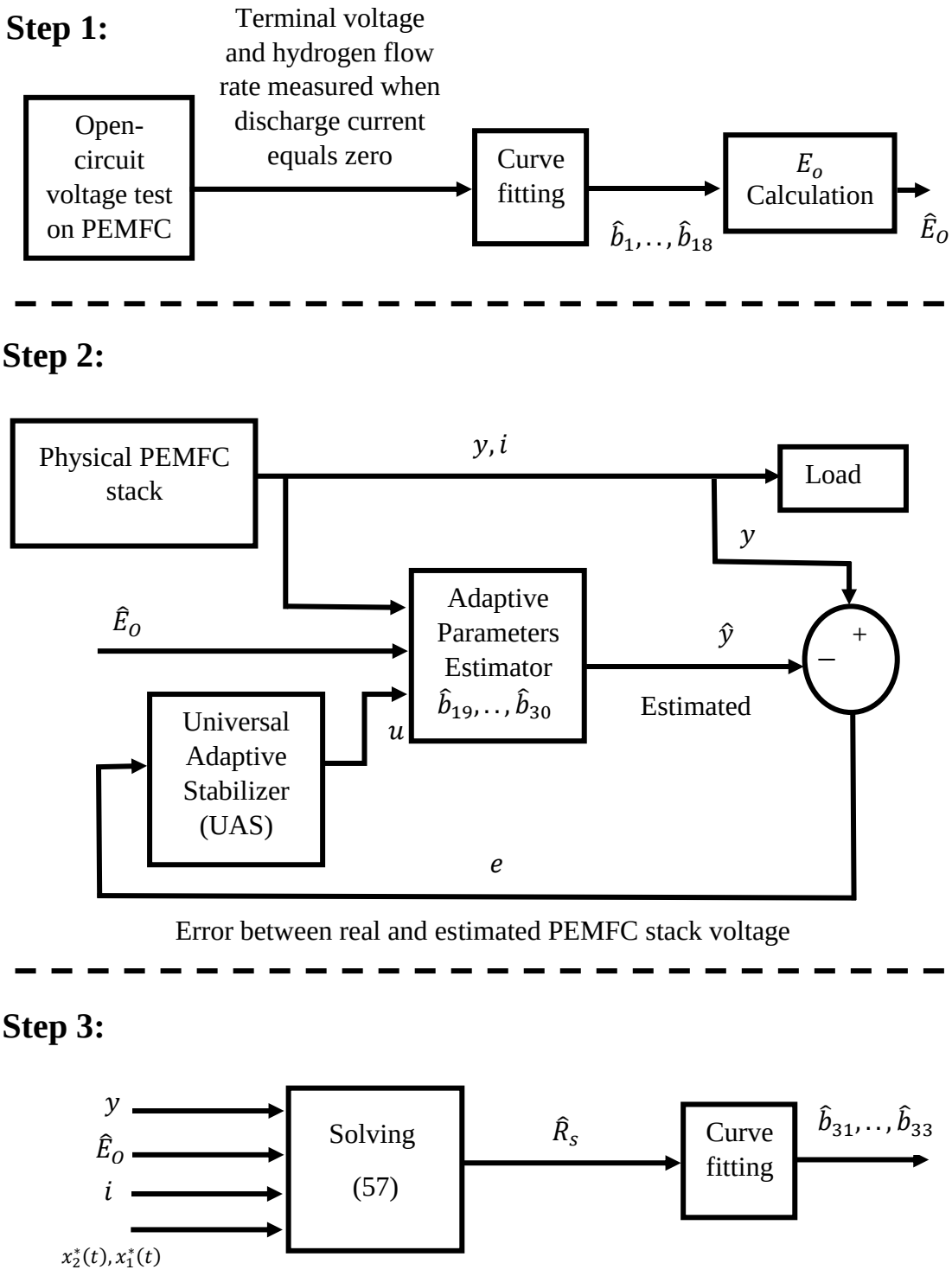

Figure 3.1: Three steps of the parameters estimation methodology for the PEMFC stack [34].

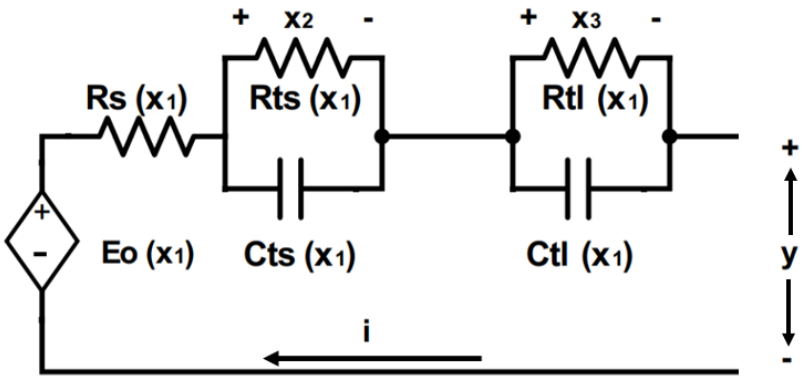

Figure 3.2: Proposed equivalent electric circuit model of a PEMFC stack.

3.2. Experimental Setup

The experimental setup is designed to extract real data to estimate all the parameters of the equivalent electrical circuit elements offline, by collecting and saving the data for later use. This experimental setup consists of three main components which are: hydrogen supply, monitoring, and measurement, two PEMFC stack systems (200-W and 30-W), and data acquisition circuitry. The hydrogen is supplied from a small carbon fiber hydrogen cylinder to the 200-W PEMFC stack. The specifications of the hydrogen cylinder are given in Table 3.1.

Table 3.1: Hydrogen external tank specifications [44].

Type	Carbon Fiber Hydrogen Gas Cylinder
Pressure Range	Up to 300 bars
Hydrogen Capacity	0.5 L to 12 L
Dimensions	102 mm × 385 mm

For the 30-W PEMFC stack, the hydrogen is supplied by water electrolysis. A PEM electrolyzer is used for hydrogen production by electrolysis of water which is the reverse reaction of the one occurring in a fuel cell. Water is split into oxygen, protons, and electrons on the anode, by applying a DC voltage (higher than the theoretical thermodynamics voltage produced from the reverse reaction, i.e. 1.482 V). The protons pass through the membrane and combine with electrons to form hydrogen on the cathode side, which can be stored in a tank. Similar to a PEMFC stack, commercial

PEM electrolyzer consists of several cells connected in series to form a stack, and they are made from the same materials [4]. In this work, Hydrofill Pro and Hydrostik Pro (metal hydride canister) are used as a PEM electrolyzer and hydrogen storage cartridge, respectively. They are manufactured by Horizon Fuel Cell Technologies [45]. The Hydrofill system is designed to refill the Hydrostik automatically with 99.99% pure dry hydrogen using distilled water. The Hydrostik is made of an aluminum alloy materials enclosure and AB2 alloy for hydrogen absorption. Therefore, the hydrogen is stored safely in a non-compressed and solid metallic form [46]. Charging one Hydrostik using the Hydrofill takes 7-8 hours approximately. The hydrogen equipment is shown in Figure 3.3. Also, the specifications of the Hydrostik and Hydrofill are given in Table 3.2 and Table 3.3, respectively.

Figure 3.3: Hydrogen equipment including distilled water, Hydrofill and Hydrostiks.

Table 3.2: Hydrostik Pro specifications [47].

Type	Horizon Hydrostik Pro
Hydrogen Capacity	10 L
Weight	105 g
Dimensions	22 mm × 88 mm
Storage Material	AB5 metal hydride
Rated Charging Pressure	30 bar
Working Temperature	0-55 ºC

Table 3.3: Hydrofill Pro specifications [46].

Type	PEM electrolysis cell
Dimensions	145 mm × 153 mm × 208 mm
Weight	1.8 kg ± 5%
Rated Power	≤ 23W
Input Voltage	10-19 V DC
Water Input	De-ionized or Distilled Water
Working Temperature	10-40 ºC
Water Consumption	Approx. 20 mL/hr
Hydrogen Output Pressure	0-30 bar
Hydrogen Generation Capacity	Up to 3 L/hr
Hydrogen Purity	99.99%

A UC800 pressure transmitter is used to measure the pressure of hydrogen supplied to the PEMFC stack provided with explosion-proof housing for safe operation, manufactured by Xi'an Yunyi Instrument Co., Ltd. [48]. The specifications are given in Table 3.4. A MEMS volume flow meter (Model MF4001) is used to measure the hydrogen flow rate, manufactured by Siargo Ltd. [49] and the specifications are shown in Table 3.5. Both digital sensors are shown in Figure 3.4, and it is recommended to calibrate them using nitrogen gas.

Hydrogen is colorless, odorless, and flammable substance and it is highly combustible in the presence of oxygen. Therefore, the tubes must be connected tightly to avoid any leak and the ventilation slots must be clear, and unobstructed during experiment operation [50]. Therefore, the NTM alarm system shown in Figure 3.5 is used to detect the hydrogen leakage and response to a low level of hydrogen in the ambient air. This alarm system is manufactured by NTM sensor, and the specifications are shown in Table 3.6 [51]. The system produces an audible and visual alarm when the hydrogen concentration levels are within the lower flammability limit (LFL). By this, the safety will be insured while running the experiments to avoid any hydrogen-related accidents in the laboratory.

Table 3.4: UC800 pressure transmitter specifications [48].

Pressure Range	0-0.6 bar
Pressure Type	Gauge, absolute, sealed gauge
Accuracy	± 0.25%
Operating Temperature Range	-20-80 ºC
Storage Temperature Range	-40-120 ºC
Power Supply	15-30 VDC
Output Signal	4-20 mA
Pressure Port	M20×1.5
Material	1Cr 18Ni 9Ti stainless steel
Diaphragm Material	316L
O-ring	Fluor rubber
Electrical Housing	Cast aluminium alloy
Insulation Resistance	100 MΩ, 100 VDC

Table 3.5: MEMS volume flow meter specifications [49].

Flow Range	0-1000 SLPM
Accuracy	± 1.5%
Power Consumption	≤50 mW
Operating Temperature Range	-10-55 ºC
Temperature Coefficient	±0.12 %/ ºC
Power Supply	8-24 VDC
Output Signal	Linear, Analog 0.5-4.5 VDC
Mechanical connection	V-nozzle
Weight	15 g
Maximum Pressure Rating	5 bar
Maximum Pressure Loss	0.0003 bar

Figure 3.4: Hydrogen pressure and flow rate digital sensors.

Table 3.6: NTM alarm system specifications [51].

Hydrogen Range in Air	0.25-4%
Voltage Input (DC)	10-57.6 VDC
Voltage Input (AC)	90-264 VAC
Maximum Switching Voltage (DC)	28 VDC
Maximum Switching Voltage (AC)	277 VAC
Rated Current	10 A
Output (sensing range)	1-4.5 VDC
Error State (output signal)	0.5 VDC
Power Consumption (25 ºC)	0.1-0.15 A
Response Time	5 seconds
Recovery Time	5 seconds
Ambient Temperature	-20-80 ºC
Relative Humidity	5-95%
Linear Flow Rate	0.02-5 m/s
Display Dimensions	133.35 mm × 120.65 mm × 35.56 mm
Sensor Module Dimensions	73.66 mm × 69.85 mm × 25.4 mm

Figure 3.5: NTM hydrogen alarm system [51].

A 200-W PEMFC stack is used to extract the parameters and validate the proposed model. It is manufactured by HES Energy Systems [52] and is shown in Figure 3.6. The 200-W PEMFC stack system contains 35 cells connected in series (12.6×12×10.7 cm^3, 500 grams, 50% efficiency). Inside the stack, there is a controller that controls purging the impurity accumulation in the anode channel. The fan is used for cooling and taking in air, an acceptable substitute for pure oxygen, from the environment to be supplied to the cathode. While the hydrogen is stored in an external tank (carbon fiber cylinder), connected by a pressure regulator to the stack. The inlet hydrogen pressure is regulated to be between 0.45-0.55 bar. The specifications of the 200-W PEMFC stack are listed in Table 3.7.

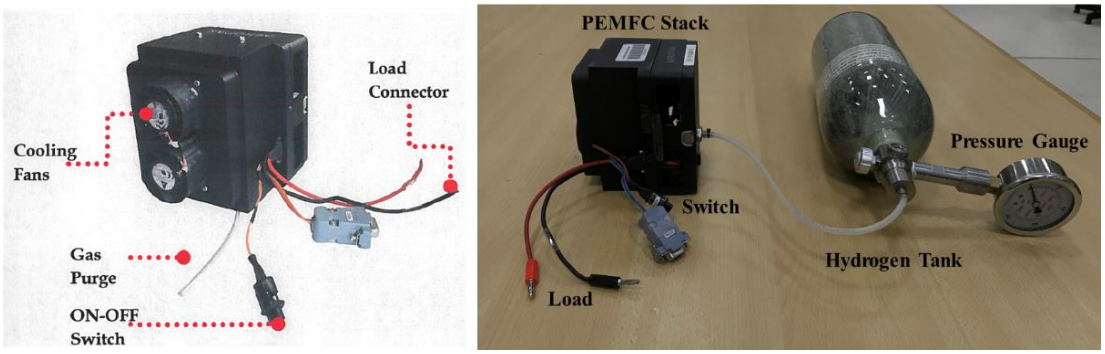

Figure 3.6: 200-W PEMFC stack system [52].

The dSPACE DS 1104 control board is used to acquire the PEMFC stack discharge data, through calibrated voltage (0-32 V), current (ACS712ELC-20A), and flow rate sensors. Also, the pulse width modulation (PWM) signal generated by a computer and connected through the dSPACE board, is fed to a relay (N020A/NC-10A)

that is connected to a load, to perform the pulse discharge test that will be discussed in the model validation section in chapter 4. A bulb (2.5 A) and different power resistances with different ratings are used in parallel and series combination, to get the desired discharge currents at different loads. The complete experimental setup is shown in Figure 3.7 along with the experiment circuit diagram in Figure 3.8. The pressure and flow rate sensors are connected between the hydrogen tank and the PEMFC stack's hydrogen inlet. Current and voltage sensors are connected to the load. The analog-to-digital converter (ADC) modules in the dSPACE DS 1104 board reads the information from the calibrated sensors. While a digital-to-analog converter (DAC) is used to provide PWM output signals to control the relay. The real-time data acquisition continues until the hydrogen tank is is fully exhausted. The data collected is to be used to identify the parameters of the PEMFC stack's model, as discussed in section **3.3**.

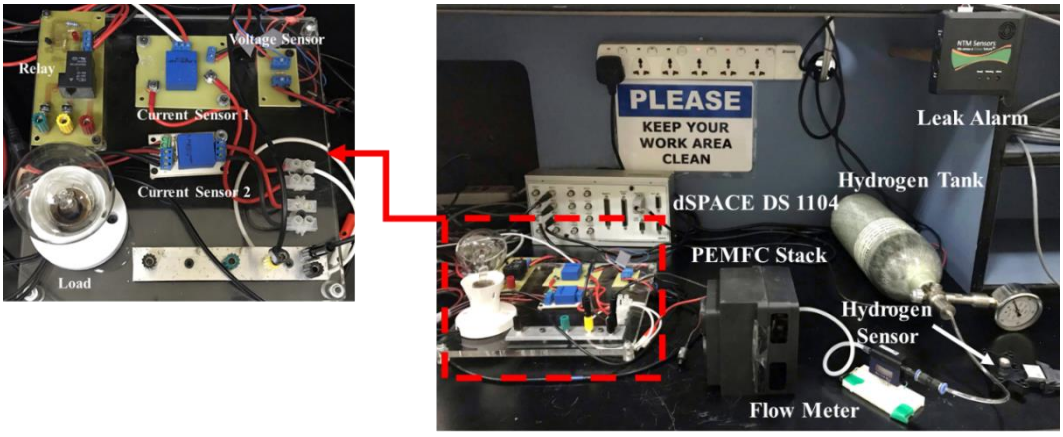

Figure 3.7: 200-W PEMFC stack experimental setup.

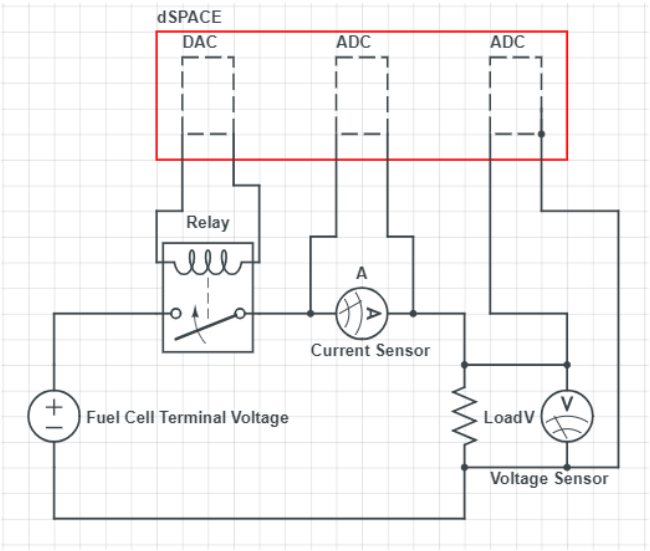

Figure 3.8: Experimental circuit diagram.

Table 3.7: 200-W PEMFC stack specifications [44].

No. of Cells	35
Rated Performance	10 A@21 V
Continuous Output Power	200 W
Output Voltage Range	21-32 V
Design Lifetime	500 h
Weight	500 g
Rated Hydrogen Consumption	3 L/min
Operating Temperature Range	0-35 ºC
Low Voltage Shutdown	20 V
Humidification	Self-humidified
Cooling	Air (integrated fan)

A 30-W PEMFC stack is also used to validate the proposed model structure, and the APE methodology for estimating the parameters, across fuel cells of different sizes. This PEMFC stack is shown in Figure 3.9 that is manufactured by Horizon Fuel Cell Technologies [45]. The specifications are given in Table 3.8. The PEMFC stack system contains 14 cells (30-W, 8×4.7×7.5 cm^3, 280 grams, 40% efficiency), a controller that controls the purging in the stack, a purge valve that manages the purging time for purging water and reductant hydrogen from the PEMFC stack, and tubes for connecting the pressure regulator and purge valve to the stack. The pressure regulator sets the pressure coming from the Hydrostik Pro (metal hydride canister) to be between 0.45-0.55 bar [53]. A Hydrofill Pro unit is used to refill the Hydrostik automatically with 99.99% pure dry hydrogen using distilled water. Similarly, the experimental setup for the 30-W fuel cell is shown in Figure 3.10. The Hydrostik is connected to UC800 pressure transmitter to measure the pressure of hydrogen supplied to the PEMFC stack. The other components are the same as the experimental setup for the 200-W PEMFC stack.

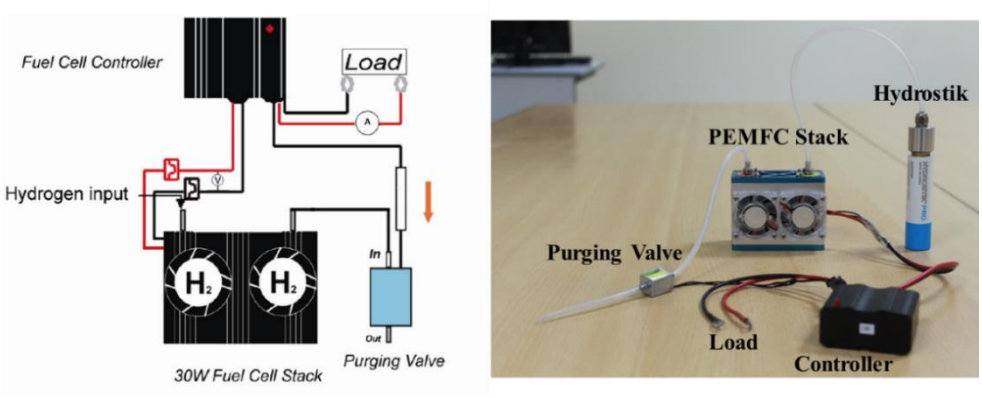

Figure 3.9: 30-W PEMFC stack system [53].

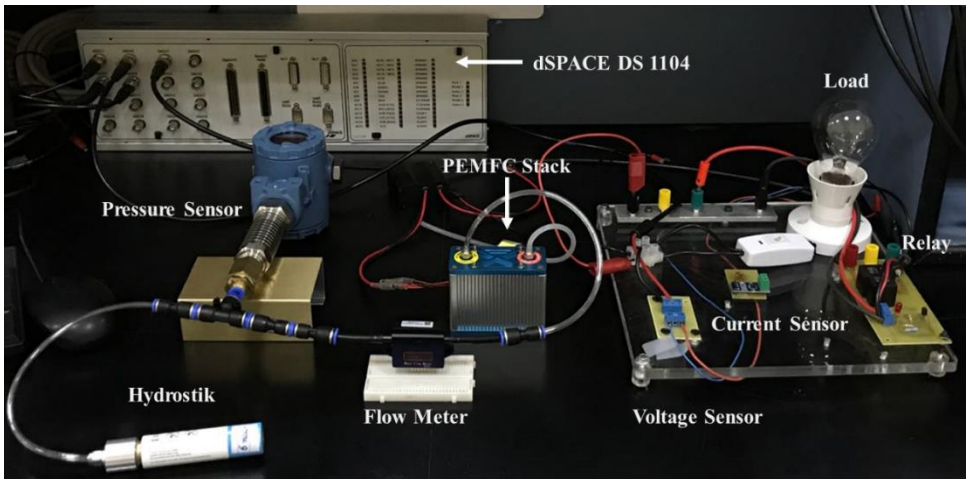

Figure 3.10: 30-W PEMFC stack experimental setup.

Table 3.8: 30-W PEMFC stack specifications [44].

No. of Cells	14
Rated Performance	3.6 A@8.4 V
Continuous Output Power	30 W
Output Voltage Range	10-14 V
Dimensions	8 cm × 4.7 cm × 7.5 mm
Weight	280 g
Rated Hydrogen Consumption	0.42 L/min
Operating Temperature Range	5-30 ºC
Low Voltage Shutdown	20 V
Humidification	Self-humidified

All measurements are taken every 0.01 seconds until the hydrogen tank is fully exhausted. It is observed that purging of the water and other impurities happens periodically every 0.5 seconds for both the 30-W and 200-W PEMFC stacks. This purging action causes a voltage drop. Therefore, it is important to filter out this voltage drop to get a smoother curve of the voltage with time or vs. the normalized hydrogen flow rate. This is done using the low pass filter (LPF) shown below:

$$G_c(s) = \frac{2\pi f}{s + 2\pi f} \tag{47}$$

where f is the frequency. For discrete time implementation the above transfer function is discretized with a time step of 1×10^{-3} second. Figure 3.11 shows a zoomed in version of the 200-W PEMFC stack's open-circuit voltage drop caused by the purging. The data are filtered using the LPF mentioned in equation (47) and is shown in Figure 3.12.

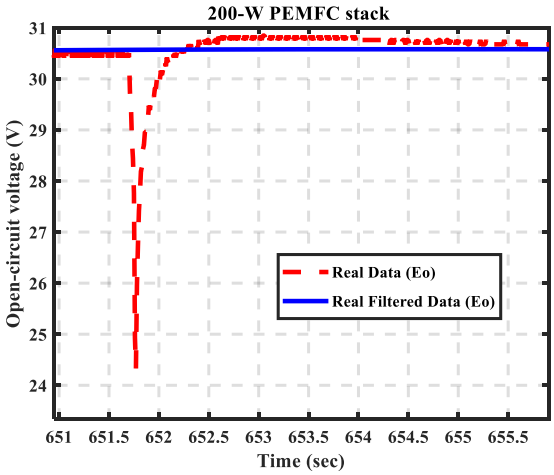

Figure 3.11: Purging effect on the 200-W PEMFC's open-circuit voltage.

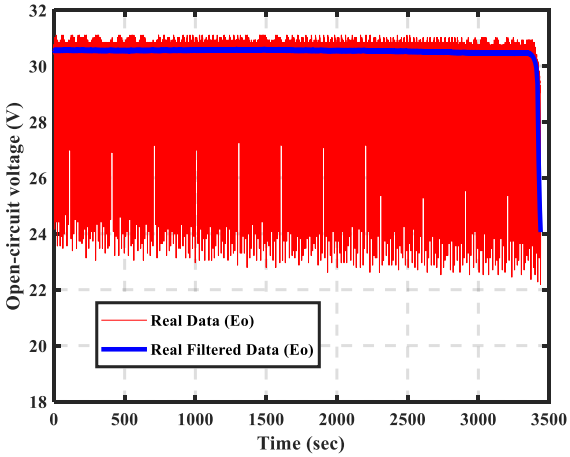

Figure 3.12: 200-W open-circuit voltage vs. time data before and after filtering.

3.3. Model Parameters Estimation

The model parameter estimation is done in three main steps that are summarized in Figure 3.1. The first step is to estimate a suitable equation for the open-circuit voltage followed by estimation of parameters needed in such an equation. The parameters of the two RC parallel combinations are estimated in the second step using the UAS-based APE methodology. In the end, the parameters of the series resistance are estimated as in step three. The detail of the three steps are explained as follow:

3.3.1. Open-circuit voltage. The first step in the model parameters estimation is to find a suitable equation for the open-circuit voltage of a PEMFC stack as a function of the normalized hydrogen flow rate. The data of the 200-W PEMFC stack are obtained by connecting no-load to the fuel cell stack and taking the measurements of the voltage and hydrogen flow rate every 0.01 seconds. Four open-circuit voltage tests are conducted so that the average value of the open-circuit voltage can be considered. As shown in Figure 3.13, the shape of open-circuit voltage of the 200-W PEMFC stack as a function of the normalized hydrogen flow rate is different from the one of a Li-ion battery as a function of the SoC. Due to this disparity, equation (13) from the CM model is not suited to describe the open-circuit voltage of a PEMFC stack in terms of the normalized hydrogen flow rate. So, a different relation for a PEMFC stack's open-circuit voltage vs. normalized hydrogen flow rate is obtained, by fitting the real open-circuit voltage values to the normalized hydrogen flow rate ($x_1(t)$), using the curve fitting toolbox in MATLAB. Many families of functions are available in the curve fitting toolbox.

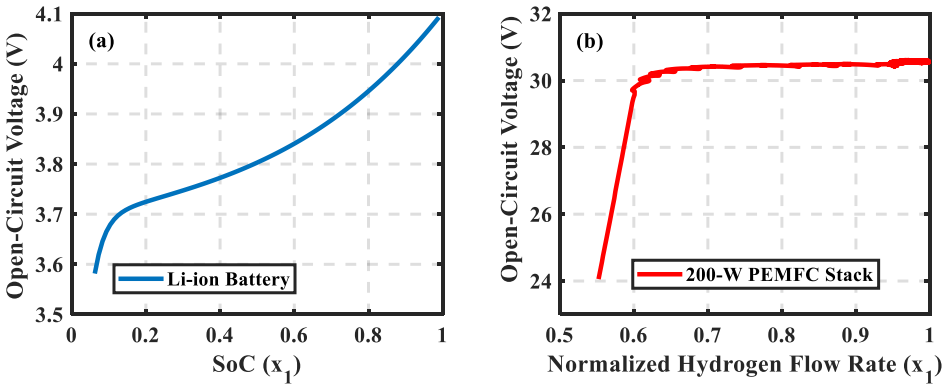

Figure 3.13: Open-circuit voltage of a Li-ion battery vs. SoC obtained from the CM model in (a), and real open-circuit voltage vs. normalized hydrogen flow rate of the 200-W PEMFC stack in (b).

Some of the fitted functions for the PEMFC stack's open-circuit voltage with their average absolute voltage errors are shown in Table 3.9, and in Figure 3.14. The average absolute voltage error $V_{avg-error}$ is calculated from (48), for the entire period of time,

$$V_{avg-error} = avg_{[t_o,T]}\left|E_o(x_1(t)) - \hat{E}_o(x_1(t))\right| \tag{48}$$

where $E_o(x_1(t))$ is the real open-circuit voltage, and $\hat{E}_o(x_1(t))$ is the open-circuit voltage obtained from the estimated equation, at each time step. The initial time is t_o and the overall period for which the open-circuit voltage measurements are recorded is T. The measurements are continued until the hydrogen tank is fully exhausted.

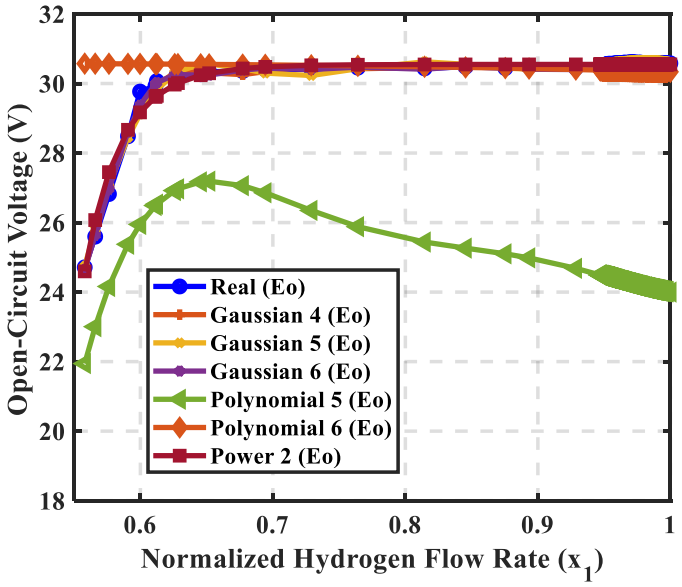

Figure 3.14: The real open-circuit voltage and the estimated open-circuit voltage, for the 200-W PEMFC stack, for each equation in Table 3.9.

As illustrated in Table 3.9, the Gaussian function with 6 terms, (52), has the minimum average absolute voltage error, which is only 20.9-mV. The estimated parameters $[\hat{b}_1 \ldots \hat{b}_{18}]$ for equation (52) are given in Table 3.10. Figure 3.15 shows the real open-circuit voltage and the estimated open-circuit voltage vs. the normalized hydrogen flow rate, along with the voltage error vs. time plot. The error is the difference between the real open-circuit voltage and the estimated open-circuit voltage. The error range is approximately between -0.25 to 0.55 V. Therefore, Gaussian function with 6 terms gives good agreement with the real data.

Table 3.9: Different estimated relations for the open-circuit voltage of a PEMFC stack with their average absolute open-circuit voltage estimation error.

Type	Function	$V_{avg-error}$ (mV)
Gaussian (4 terms)	$\hat{E}_o(x_1) = \hat{b}_1 e^{\left(-\frac{x_1-\hat{b}_2}{\hat{b}_3}\right)^2} + \hat{b}_4 e^{\left(-\frac{x_1-\hat{b}_5}{\hat{b}_6}\right)^2} + \hat{b}_7 e^{\left(-\frac{x_1-\hat{b}_8}{\hat{b}_9}\right)^2} + \hat{b}_{10} e^{\left(-\frac{x_1-\hat{b}_{11}}{\hat{b}_{12}}\right)^2}$	29.5
Gaussian (5 terms)	$\hat{E}_o(x_1) = \hat{b}_1 e^{\left(-\frac{x_1-\hat{b}_2}{\hat{b}_3}\right)^2} + \hat{b}_4 e^{\left(-\frac{x_1-\hat{b}_5}{\hat{b}_6}\right)^2} + \hat{b}_7 e^{\left(-\frac{x_1-\hat{b}_8}{\hat{b}_9}\right)^2} + \hat{b}_{10} e^{\left(-\frac{x_1-\hat{b}_{11}}{\hat{b}_{12}}\right)^2} + \hat{b}_{13} e^{\left(-\frac{x_1-\hat{b}_{14}}{\hat{b}_{15}}\right)^2}$	69.3
Gaussian (6 terms)	$\hat{E}_o(x_1) = \hat{b}_1 e^{\left(-\frac{x_1-\hat{b}_2}{\hat{b}_3}\right)^2} + \hat{b}_4 e^{\left(-\frac{x_1-\hat{b}_5}{\hat{b}_6}\right)^2} + \hat{b}_7 e^{\left(-\frac{x_1-\hat{b}_8}{\hat{b}_9}\right)^2} + \hat{b}_{10} e^{\left(-\frac{x_1-\hat{b}_{11}}{\hat{b}_{12}}\right)^2} + \hat{b}_{13} e^{\left(-\frac{x_1-\hat{b}_{14}}{\hat{b}_{15}}\right)^2} + \hat{b}_{16} e^{\left(-\frac{x_1-\hat{b}_{17}}{\hat{b}_{18}}\right)^2}$	**20.9**
Polynomial (5 terms)	$\hat{E}_o(x_1) = \hat{b}_1 x_1^5 + \hat{b}_2 x_1^4 + \hat{b}_3 x_1^3 + \hat{b}_4 x_1^2 + \hat{b}_5 x_1 + \hat{b}_6$	6208.6
Polynomial (6 terms)	$\hat{E}_o(x_1) = \hat{b}_1 x_1^6 + \hat{b}_2 x_1^5 + \hat{b}_3 x_1^4 + \hat{b}_4 x_1^3 + \hat{b}_5 x_1^2 + \hat{b}_6 x_1 + \hat{b}_7$	212.8
Power (2 terms)	$\hat{E}_o(x_1) = \hat{b}_1 x_1^{\hat{b}_2} + \hat{b}_3$	37.6

Table 3.10: Open-circuit voltage relation parameters using Gaussian with 6 terms for 200-W PEMFC stack.

Parameter	$\hat{b}_1$	$\hat{b}_2$	$\hat{b}_3$	$\hat{b}_4$	$\hat{b}_5$	$\hat{b}_6$
Value	37.66	0.8312	0.564	-12.02	0.7197	0.2646
Parameter	$\hat{b}_7$	$\hat{b}_8$	$\hat{b}_9$	$\hat{b}_{10}$	$\hat{b}_{11}$	$\hat{b}_{12}$
Value	0.7794	0.8587	0.05231	5.262	0.7369	0.1027
Parameter	$\hat{b}_{13}$	$\hat{b}_{14}$	$\hat{b}_{15}$	$\hat{b}_{16}$	$\hat{b}_{17}$	$\hat{b}_{18}$
Value	2.678	0.6705	0.05097	6.09	0.6028	0.05159

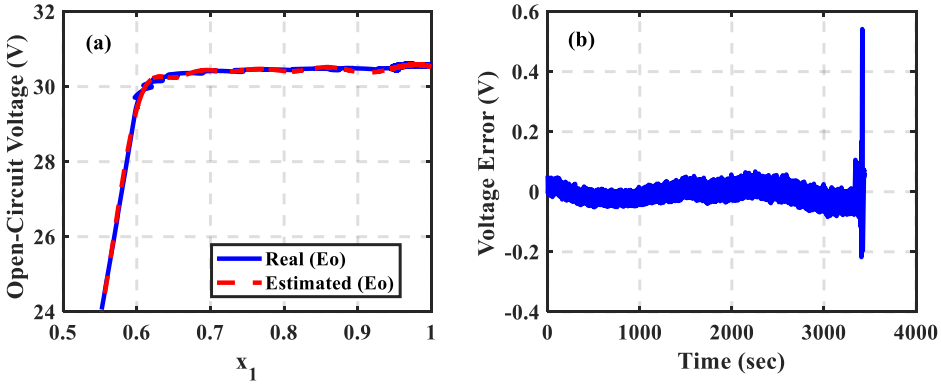

Figure 3.15: Real open-circuit voltage of the 200-W PEMFC stack vs. the estimated open-circuit voltage with 20.9-mV average absolute voltage error in (a), and the voltage error vs. time in (b).

3.3.2. Terminal voltage dynamics. Like the CM battery model, the PEMFC stack has the same voltage drop characteristics. Therefore, the APE discussed in section **2.3** has been applied to estimate the terminal voltage of the PEMFC stack using UAS-based observer (31)-(34). The UAS is a special type of adaptive control strategy used to meet predetermined control objective for a given class of systems. Here the objective is tuning the values of the elements in the two RC parallel combinations, used in the proposed equivalent circuit model of a PEMFC stack, until the error between the estimated terminal voltage ($\hat{y}$) and the real terminal voltage (y) is negligibly small. In this technique, Mittag-Leffler function, (19), is used as a Nussbaum function to design the UAS for the model parameters estimation. This is because it has a very fast growth rate in the positive and negative direction, and hence provides high speed for the error convergence to zero. In the observer model, (49)-(57), the control signal $u(t)$ is added to prove that the error between the real and estimated terminal voltage leads to zero. A modification of the observer model in (21)-(30) has been done. This is because the number of parameters for the PEMFC stack is higher than the parameters of the battery. Also, the functions of the open-circuit voltage and the series resistance are different. As mentioned before, the values of the hydrogen flow rate are normalized from 0 to 1 and used as x_1.

$$\dot{\hat{x}}_2(t) = -\frac{\hat{x}_2(t)}{\hat{R}_{ts}(x_1)\hat{C}_{ts}(x_1)} + u(t), \hat{x}_2 \geq 0 \qquad (49)$$

$$\dot{\hat{x}}_3(t) = -\frac{\hat{x}_3(t)}{\hat{R}_{tl}(x_1)\hat{C}_{tl}(x_1)} + u(t), \hat{x}_3 \geq 0 \tag{50}$$

$$\hat{y}(t) = \hat{E}_o(x_1) - \hat{x}_2 - \hat{x}_3 \tag{51}$$

$$\begin{aligned}\hat{E}_o(x_1) = \hat{b}_1 e^{\left(-\frac{x_1-\hat{b}_2}{\hat{b}_3}\right)^2} + \hat{b}_4 e^{\left(-\frac{x_1-\hat{b}_5}{\hat{b}_6}\right)^2} + \hat{b}_7 e^{\left(-\frac{x_1-\hat{b}_8}{\hat{b}_9}\right)^2} \\ + \hat{b}_{10} e^{\left(-\frac{x_1-\hat{b}_{11}}{\hat{b}_{12}}\right)^2} + \hat{b}_{13} e^{\left(-\frac{x_1-\hat{b}_{14}}{\hat{b}_{15}}\right)^2} + \hat{b}_{16} e^{\left(-\frac{x_1-\hat{b}_{17}}{\hat{b}_{18}}\right)^2}\end{aligned} \tag{52}$$

$$\hat{R}_{ts}(x_1) = \hat{a}_{19} e^{-\hat{a}_{20} x_1} + \hat{a}_{21} \tag{53}$$

$$\hat{R}_{tl}(x_1) = \hat{a}_{22} e^{-\hat{a}_{23} x_1} + \hat{a}_{24} \tag{54}$$

$$\hat{C}_{ts}(x_1) = -\hat{a}_{25} e^{-\hat{a}_{26} x_1} + \hat{a}_{27} \tag{55}$$

$$\hat{C}_{tl}(x_1) = -\hat{a}_{28} e^{-\hat{a}_{29} x_1} + \hat{a}_{30} \tag{56}$$

Similar methodology to the one presented in **Algorithm 1** is used to obtain the parameters $[\hat{b}_{19} \ldots \hat{b}_{30}]$ adaptively using the same a_{nu}, a_{nl}, λ_{x_n}, and λ_{y_n} used to estimate the battery parameters in [34]. **Algorithm 2** represents the modification of **Algorithm 1**. Also, **Lemma 1** for the battery is modified to **Lemma 2**. To estimate the parameters, a constant discharge current curve at 0.25 A of PEMFC stack's terminal voltage is used. The data of the 200-W PEMFC stack are obtained by connecting the desired load (0.25 A) to the fuel cell stack and taking the measurements of the voltage and hydrogen flow rate every 0.01 seconds. The measurements are continued until the hydrogen tank is fully exhausted.

The procedure of the APE process is summarized in **Algorithm 2**. In **Algorithm 2**, all the physical requirements, inputs, initial conditions, and output are summarized in pseudocode form. Equation (57) is used to estimate parameters from $\hat{b}_{19}$ to $\hat{b}_{19}$ at each time step (0.01 second) to get the values of $\hat{R}_{ts}$, $\hat{R}_{tl}$, $\hat{C}_{ts}$, and $\hat{C}_{tl}$.

$$\begin{gathered}\dot{\hat{b}}_n(t) = e^2(t) + \lambda_{x_n}\left(b_{nu} - \hat{b}_n(t)\right) + \lambda_{y_n}\left(b_{nl} - \hat{b}_n(t)\right), \\ \hat{b}_n > 0 \; for \; n \in \{19,20, \ldots.,30\}.\end{gathered} \tag{57}$$

At each time step, the real terminal voltage is subtracted from the estimated terminal voltage to compute the error signal e. The error is used to obtain the values of

the estimated parameters as in (57), and to compute the control signal u by (34). The control signal tries to drive the error to zero. The values of $\hat{b}_n$ are returned if e is within a pre-set small bound and **Lemma 2** conditions are satisfied. Else, a null-values are returned. At the end of the APE process (when e converges to zero), the last non-null values of $\hat{b}_n$ represent the valid estimated values of the parameters [$\hat{b}_{19}$,…, $\hat{b}_{30}$]. These parameters are used to calculate the two RC parallel combinations via (53)-(56). All the upper bound, lower bound, user's confidence, initial values, and the valid estimated values of the parameters are listed in Table 3.11. The values of the parameters are similar to the parameters obtained in the CM model for a Li-ion battery.

Table 3.1: Estimated parameters of the two RC parallel combinations.

Parameter	Upper bound (b_{nu})	Lower bound (b_{nl})	λ_{x_n}	λ_{y_n}	Initial value	Estimated value
$\hat{b}_{19}$	1	0.1	50	50	180	0.55
$\hat{b}_{20}$	50	10	50	50	500	30
$\hat{b}_{21}$	0.1	0.01	50	50	24	0.055
$\hat{b}_{22}$	10	1	50	50	3600	5.5
$\hat{b}_{23}$	200	100	50	50	500	150
$\hat{b}_{24}$	0.1	0.01	50	50	264	0.055
$\hat{b}_{25}$	1000	500	60	55	2000	760.8698
$\hat{b}_{26}$	30	1	50	10	300	25.1667
$\hat{b}_{27}$	800	500	80	50	3000	684.6157
$\hat{b}_{28}$	7000	5000	10	10	420	6000
$\hat{b}_{29}$	50	5	50	50	162	27.5
$\hat{b}_{30}$	5000	3000	10	20	363	3666.7

Lemma 2: *Let* $n = \{25,27,28,30\}$. *Suppose* λ_{x_n}, λ_{y_n}, b_{nu}, b_{nl} *are positive real numbers. Further Let* $\mathbf{1} = [1\ 1]^T, \mathbf{\Lambda}_n = \left[\lambda_{x_n}\ \ \lambda_{y_n}\right]^T, \mathbf{P}_n = [b_{nu}\ \ b_{nl}]^T$, *then the following statements hold for* $x_1(t) \in (0,1]$

1. *If* $0 < \hat{b}_{27}(t_{initial}) < \hat{b}_{25}(t_{initial})$, $\mathbf{1}^T\mathbf{\Lambda}_{27} > \mathbf{1}^T\mathbf{\Lambda}_{25}$, $\mathbf{P}_{27}^T\,\mathbf{\Lambda}_{27} < \mathbf{P}_{25}^T\,\mathbf{\Lambda}_{25}$, *and* $\hat{b}_{26}(t) > -\frac{1}{x_1(t)}\ln\left(\frac{\hat{b}_{27}(t)}{\hat{b}_{25}(t)}\right)$, *then* $\hat{C}_{ts}\big(x_1(t)\big) > 0$
2. *If* $0 < \hat{b}_{30}(t_{initial}) < \hat{b}_{28}(t_{initial})$, $\mathbf{1}^T\mathbf{\Lambda}_{30} > \mathbf{1}^T\mathbf{\Lambda}_{28}$, $\mathbf{P}_{30}^T\,\mathbf{\Lambda}_{30} < \mathbf{P}_{28}^T\,\mathbf{\Lambda}_{28}$, *and* $\hat{b}_{29}(t) > -\frac{1}{x_1(t)}\ln\left(\frac{\hat{b}_{30}(t)}{\hat{b}_{28}(t)}\right)$, *then* $\hat{C}_{tl}\big(x_1(t)\big) > 0$

Proof: See [34] for proof.

Algorithm 2: Adaptive PEMFC stack parameter estimation algorithm (pseudocode)

Physical requirements: PEMFC stack, Full hydrogen tank, appropriate discharge and data acquisition circuitry, hydrogen pressure and flow rate sensors.

Inputs: Initial time $t_{initial}$, time step t_{step}, termination time t_{final}, parameters $\hat{b}_1, \dots, \hat{b}_{18}$ from step 1, parameters $\hat{b}_n(t_{initial})$, b_{nu}, b_{nl}, λ_{x_n}, λ_{y_n} for $n \in \{19, \dots, 30\}$ satisfying conditions require for **Lemma 2** to hold. Small positive discharge current $i(t)$ for $t \geq t_{initial}$. Adaptive tracking error bound $\epsilon_2 > 0$ (smaller values of ϵ_2 increase accuracy).

Initial conditions: $x_1(t_{initial}) = 1$, $\hat{x}_2(t_{initial}) = \hat{x}_3(t_{initial}) = 0$, $\hat{y}(t_{initial}) = y(t_{initial})$.

Outputs: Estimated PEMFC stack parameters $[\hat{b}_{19}, \dots, \hat{b}_{30}]$.

1: **for** $t = t_{initial} : t_{step} : t_{final}$ **do**
2: Read measured PEMFC stack terminal voltage y, PEMFC discharge current i
3: Read measured hydrogen pressure and flow rate and normalize it (x_1)
4: Calculate $e = y - \hat{y}$
5: Find u as per equation (34)
6: Get estimated parameters $\hat{b}_n$ according to equation (57) for $n \in \{19, \dots, 30\}$
7: Calculate $\hat{R}_{ts}$, $\hat{R}_{tl}$, $\hat{C}_{ts}$, C_{tl} using equation (53)-(56).
8: Compute state estimates $\hat{x}_2$, $\hat{x}_3$ using equations **Error! Reference source not found.** and (50)
9: Update estimated terminal voltage $\hat{y}$ using equation (51)
10: **if** $e < \epsilon_2$ and conditions in **Lemma 2** hold are satisfied **then**
11: **Return** $[\hat{b}_{19}, \dots, \hat{b}_{30}]$
12: **Continue** loop execution
13: **else**
14: **Return Null**
15: **Continue** loop execution
16: **end if**
17: **end for**

In step 3, equation (58) is used to obtain $\hat{R}_s(x_1(t))$, where x_2^* and x_3^* are the voltage drops across the two RC parallel combinations using the estimated parameters values in Table 3.11. Then, a new function for the series resistance is obtained as in equation (59) using the curve fitting techniques. The parameters $\hat{b}_{31}$, $\hat{b}_{32}$, and $\hat{b}_{33}$ are given in Table 3.12.

$$\hat{R}_s(x_1(t)) = i(t)^{-1}\left(\hat{E}_o(x_1(t)) - x_2^*(t) - x_3^*(t) - y(t)\right) \quad (58)$$

$$Where\ 0 < i(t) < \epsilon, \text{ and}$$

$$x_2^*(t) = x_2(t)|_{R_{ts}\to\hat{R}_{ts},C_{ts}\to\hat{C}_{ts}}$$
$$x_3^*(t) = x_3(t)|_{R_{tl}\to\hat{R}_{tl},C_{tl}\to\hat{C}_{tl}}$$

$$\hat{R}_s(x_1) = -\hat{b}_{31}x_1^{\hat{b}_{32}} + \hat{b}_{33} \tag{59}$$

Table 3.12: Estimated series resistance parameters at 0.25 A discharge current.

Parameter	$\hat{b}_{31}$	$\hat{b}_{32}$	$\hat{b}_{33}$
Value	0.0822	176.1	2.767

By estimating all the model parameters $[\hat{b}_1,\ldots,\hat{b}_{33}]$., the estimated terminal voltage is calculated and compared to the real terminal voltage, as shown in Figure 3.16. The average absolute terminal voltage estimation error is only 20.7-mV, computed by (60),

$$V_{avg-error} = Avg_{[t_o,T]}|y(t) - \hat{y}(t)| \tag{60}$$

where $y(t)$ is the real PEMFC stack terminal voltage and $\hat{y}(t)$ is the estimated terminal voltage obtained from the proposed model, at each time step.

As shown in Figure 3.16, the estimated terminal voltage from the proposed model and methodology gives a good agreement with the real terminal voltage. Also, the range of the error, which is the difference between the estimated and the real terminal voltages, is between -0.2 to 0.58 V only. Thus, the proposed model and parameters estimation procedure is valid and accurate for the 200-W PEMFC stack.

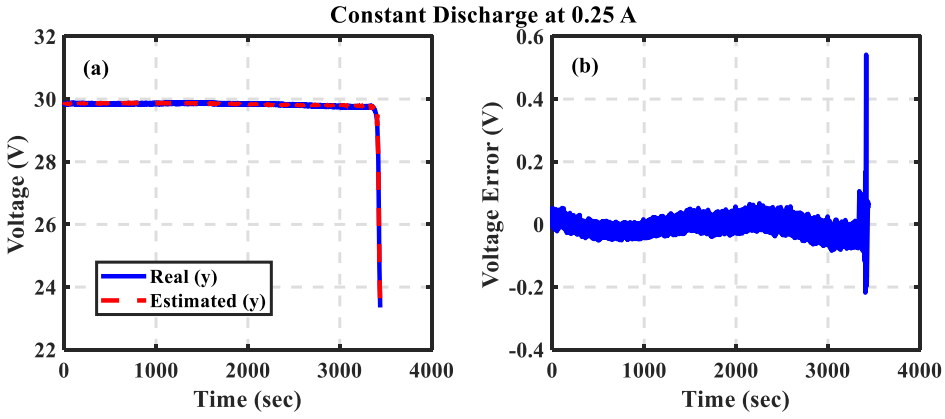

Figure 3.16: Real terminal voltage of the 200-W PEMFC stack vs. the estimated terminal voltage with 20.7-mV average absolute voltage error at 0.25 A in (a), and the voltage error vs. time in (b).

The current values with time are shown in Figure 3.17 for the 0.25 A load discharge test. The current changes slightly when the hydrogen is supplied at the maximum flow rate. Then, a sudden drop occurs when the hydrogen flow rate starts decreasing. This illustrates that there is a direct relationship between the current and the hydrogen flow rate in PEMFC stack.

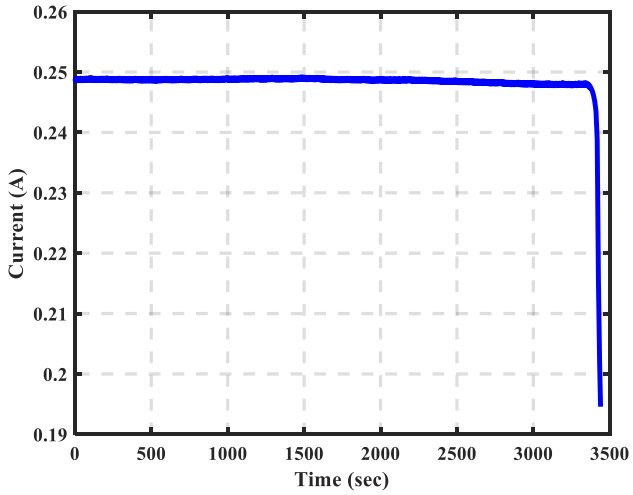

Figure 3.17: Constant discharge current at 0.25 A.

The equivalent electrical circuit elements $\hat{R}_{ts}(x_1)$ and $\hat{R}_{tl}(x_1)$ are shown in Figure 3.18, $\hat{C}_{ts}(x_1)$ and $\hat{C}_{tl}(x_1)$ are shown in Figure 3.19, and $\hat{R}_s(x_1)$ is shown in Figure 3.20. All the elements are functions of the normalized hydrogen flow rate. The values of the resistances $\hat{R}_{ts}(x_1)$, $\hat{R}_{tl}(x_1)$, and $\hat{R}_s(x_1)$ change slightly with the hydrogen flow rate. While the values of the capacitance $\hat{C}_{ts}(x_1)$ and $\hat{C}_{tl}(x_1)$ decrease at lower values of hydrogen flow rate. The proposed model accounts for the hydrogen flow rate dynamics, thus the nonlinear behavior of the PEMFC stack is captured effectively.

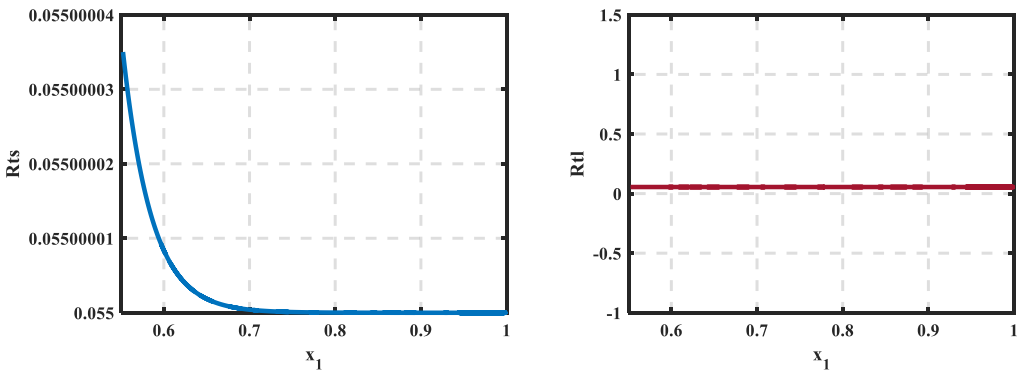

Figure 3.18: Estimated equivalent electrical circuit elements $\hat{R}_{ts}(x_1)$ and $\hat{R}_{tl}(x_1)$.

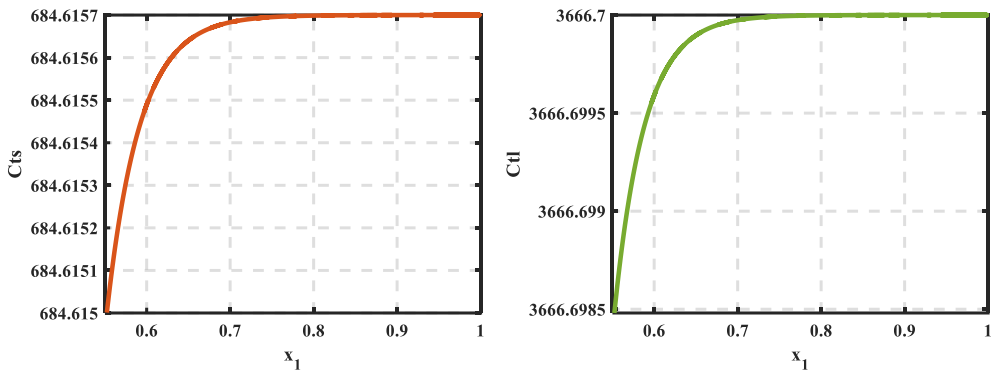

Figure 3.19: Estimated equivalent electrical circuit elements $\hat{C}_{ts}(x_1)$ and $\hat{C}_{tl}(x_1)$.

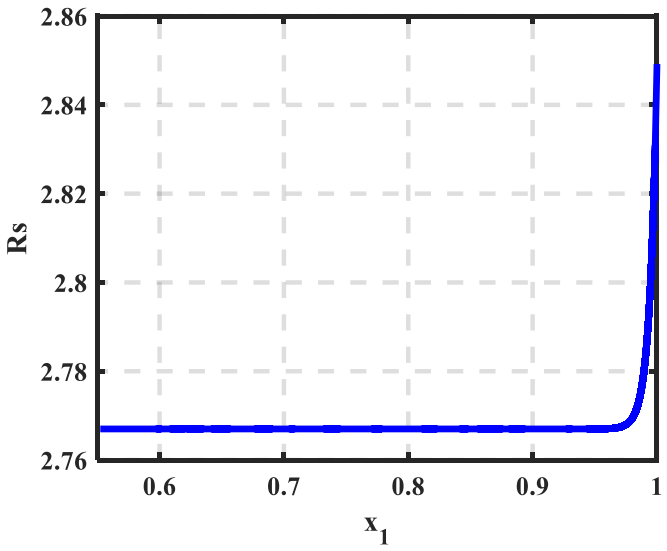

Figure 3.20: Estimated equivalent electrical circuit elements $\hat{R}_s(x_1)$.

Chapter 4. Results and Discussion

The model validation is presented in this chapter, after estimating all the model parameters using the proposed model and methodology at 0.25 A constant discharge current. The model validation tests were conducted at different constant and variable discharge currents. The estimated parameters at 0.25 A should work for all the other loads. However, it is illustrated that only the parameters values of the series resistance change at different loads, as discussed in section **4.1**. For the following experimental results, the 200-W PEMFC stack voltage and current data have been collected offline through the experimental runs and used to estimate the model parameters as the proposed steps in Figure 3.1. In addition, the model has been validated using different PEMFC stack size and from different manufacturers (30-W PEMFC stack), that shows that the proposed model and methodology are versatile and accurate. In total eleven tests are done for the model validation and studying the stack size effect.

4.1. Model Validation

The model validation is carried out under variable load conditions. For testing the proposed parameters estimation process, the following test protocols are used:

- Constant load discharge tests (4.7 A, 2.45 A, 1.73 A, 1.35 A, 0.58 A, 0.33 A and 0.25 A).
- Low pulse discharge current (0.95 A for 5 minutes and no-load for 5 minutes).
- High pulse discharge current (2.5 A for 5 minutes and no-load for 5 minutes).
- Random pulse discharge current (a combination of 0.95 A, 2.5 A and no-load).

The constant load discharge tests were carried out for six different loads at low, medium, and high current values. The real data is measured by connecting the desired load to the 200-W PEMFC stack's terminal and taking the measurements of the voltage and hydrogen flow rate until the hydrogen cylinder is fully exhausted. After collecting the real data for the terminal voltage, the estimated terminal voltage is computed by the proposed model. The real (solid lines) and the estimated (dashed lines) terminal voltages for the six different loads is shown in Figure 4.1.

The currents values are plotted in Figure 4.2. Also, the error plot for each load is shown in Figure 4.3, and the average absolute voltage errors are shown in Table 4.1. It is illustrated that the error between the real and estimated terminal voltage for each case is approximately between -0.2 to 0.5 V. The average absolute voltage error is increasing when the load is increased as shown in Table 4.2. But the estimation error is still within a reasonably small value for all the different loads. This illustrates that the proposed model and the APE methodology are valid and accurate for all the constant discharge currents cases.

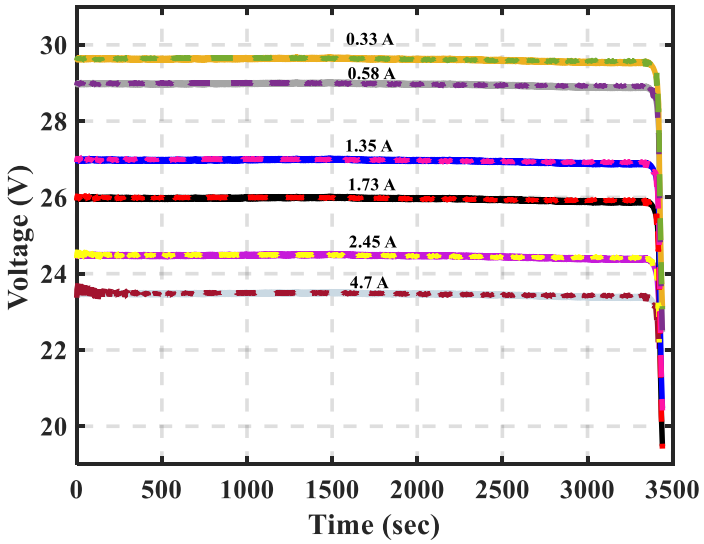

Figure 4.1: Constant load discharge validation tests, solid lines show the real voltage values while the dashed lines show the estimated voltage values.

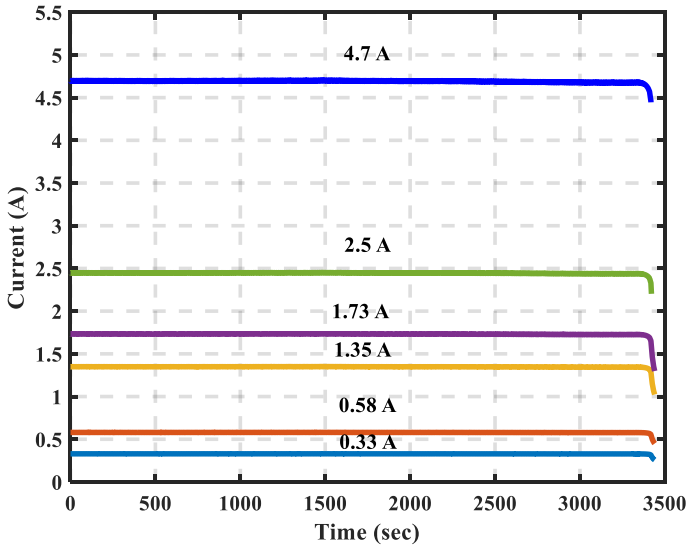

Figure 4.2: Constant load discharge currents vs. time.

Table 4.1: Average absolute voltage error at different constant loads.

Load	$V_{avg-error}(mV)$
4.7 A	23.55
2.45 A	21.49
1.73 A	21.29
1.35 A	21
0.58 A	20.73
0.33 A	20.72

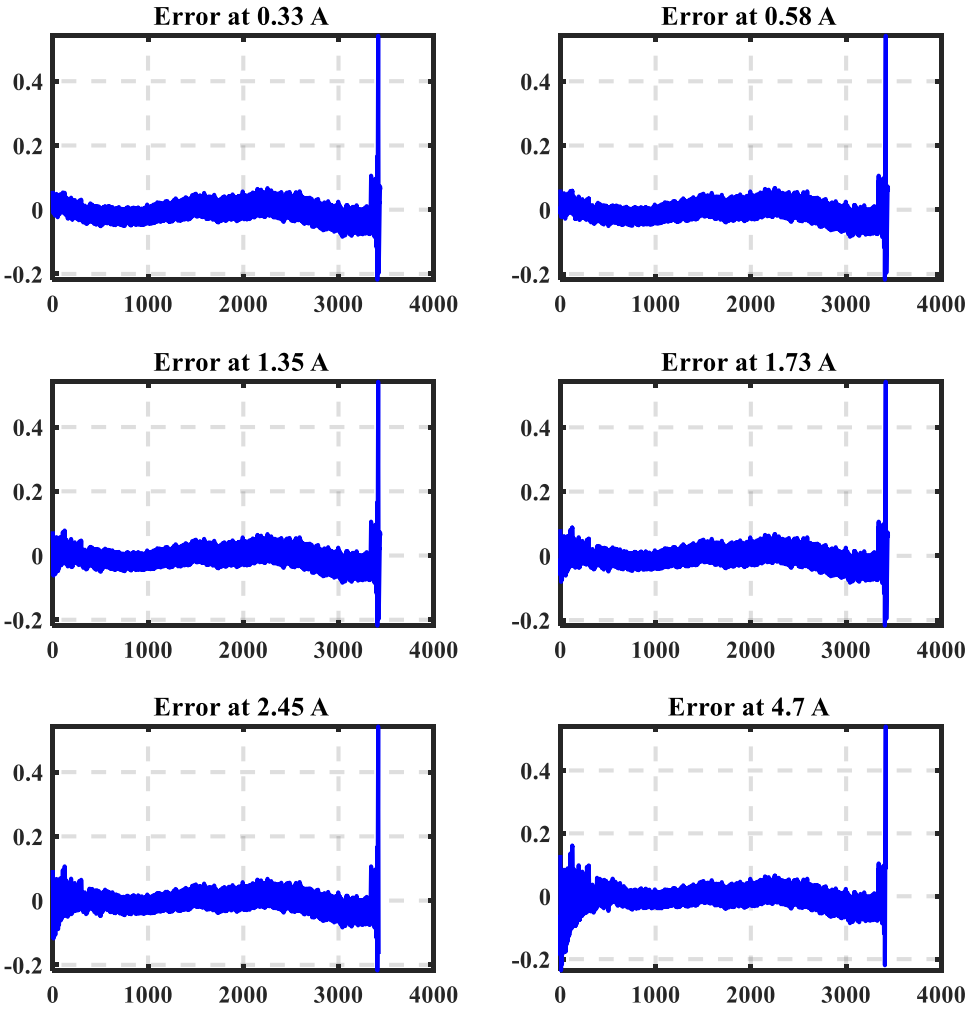

Figure 4.3: Error vs. time for different constant discharge current tests.

It is illustrated that the parameters of the open-circuit voltage and the two RC parallel combinations $[\hat{b}_1,..,\hat{b}_{30}]$ are the same as the parameters obtained at 0.25 A constant discharge current (listed in Table 3.10 and Table 3.11). However, the values of the series resistance change for different loads because $\hat{b}_{33}$ increases as the current load decreases. The values of the series resistance parameters for each current value are shown in Table 4.2. In Figure 4.4, the average series resistance is computed along the entire period of time for each current value. The series resistance average value is decreasing with increasing the current. To explain this phenomenon more tests must be conducted at different conditions. This can be investigated in further work in the future. For the 200-W PEMFC stack, only step 3 in Figure 3.1 must be done for different loads to estimate the series resistance parameters.

Table 4.2: Estimated series resistance parameters at different constant loads.

Load	$\hat{b}_{31}$	$\hat{b}_{32}$	$\hat{b}_{33}$
4.7 A	0.0822	176.1	1.441
2.45 A	0.0822	176.1	2.417
1.73 A	0.0822	176.1	2.583
1.35 A	0.0822	176.1	2.587
0.58 A	0.0822	176.1	2.661
0.33 A	0.0822	176.1	2.75

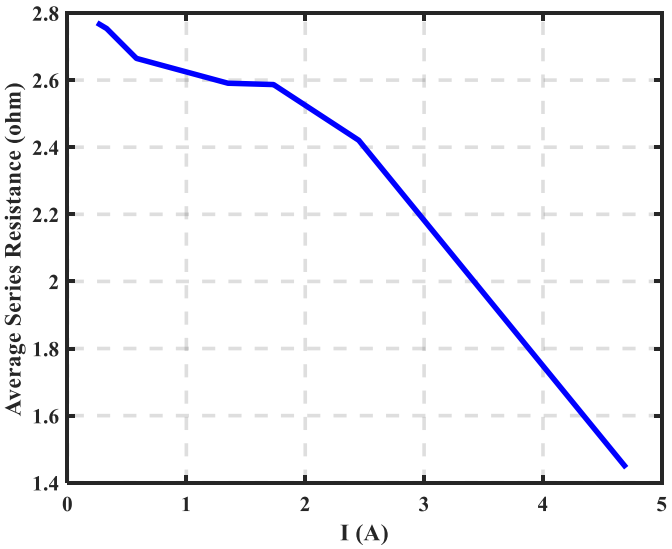

Figure 4.4: Average series resistance at different current values.

The model can predict the V-I polarization curve of a fuel cell stack as shown in Figure 4.5. This curve displays the output voltage at a given current, which is the most common method of testing the fuel cell in industry and research. The V-I polarization curve is divided into three main regions. At low current, part of the voltage is lost to overcome the activation energy needed to start the chemical reaction. Thus, the terminal voltage is less than the open-circuit voltage even if the current is relatively very small. Then, the linear region in the plot indicates the losses due to the series resistance. This ohmic loss indicated the resistance of ions flow (electrons and hydrogen protons) through the fuel cell stack components (membrane, electrodes, and electrical interconnection). At high current values, a sudden voltage drop occurs. This is because the fuel cell fails on transporting enough reactants (hydrogen and oxygen) to provide the high current. Also, the accumulation of water at the cathode side prevents the oxygen from entering and reacting with the hydrogen protons and electrons. This is known as concentration polarization.

In Figure 4.5, the real and estimated terminal voltages at different currents are shown. These values are taking from the constant discharge current tests at the maximum hydrogen flow rate (x_1=1). The estimated values give a good agreement with the real data.

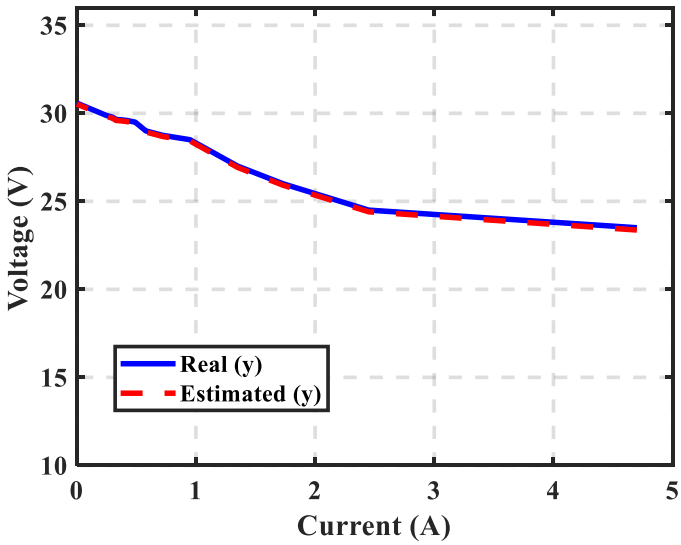

Figure 4.5: 200-W PEMFC stack V-I polarization curve at the maximum hydrogen flow rate (x_1=1).

For the pulse discharge validation, two tests are conducted at low (0.95 A) and high current values (2.5 A). The real data are obtained by connecting the desired load for 5 minutes then disconnecting it (no-load) for another 5 minutes. The switching between the load is done by feeding a PWM signal to a relay. Then, the estimated terminal voltages are obtained from the proposed model using estimated parameters $[\hat{b}_1, .., \hat{b}_{33}]$.

For the pulse load discharge test at 0.95 A, the average absolute voltage error is 50.8-mV only as shown in Figure 4.6. The error between the estimated and real terminal voltages are between -2 to 2 V. Also, the current vs. time is shown in Figure 4.7.

For the pulse load discharge test at 2.5 A, the average absolute voltage error is 75-mV as illustrated in Figure 4.8. The error between the estimated and real terminal voltages are between -6 to 6 V. It is obvious that the error increases for high current values. The current vs. time is illustrated in Figure 4.9.

In addition, the last test is done for a combination of 0.95 A, 2.5 A and open-circuit voltage (no-load) at variable time intervals. The model is also validated by this test as shown in Figure 4.10. The average absolute voltage error is 60.9-mV. The error range is between -0.1 to 0.2 V. This test shows that the model is valid for the pulse load discharge tests at high and low current values and with small estimation error. The current vs. time is shown in Figure 4.11.

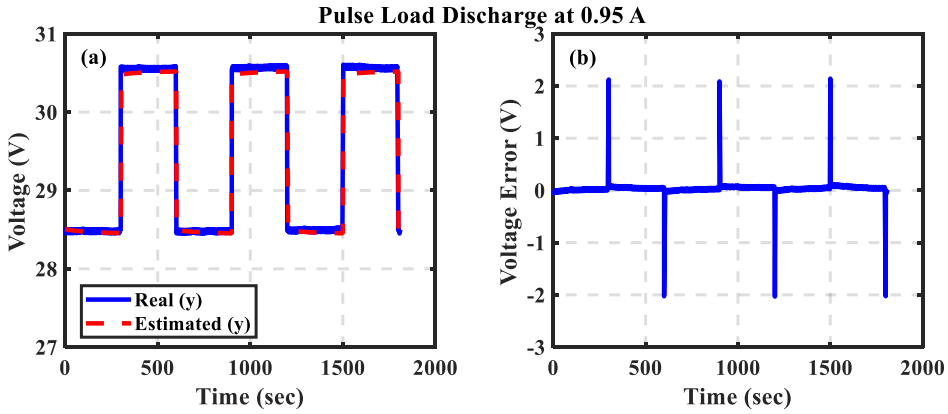

Figure 4.6: Pulse load discharge validation at 0.95 A with 50.8-mV average absolute voltage error in (a), and the voltage error vs. time in (b).

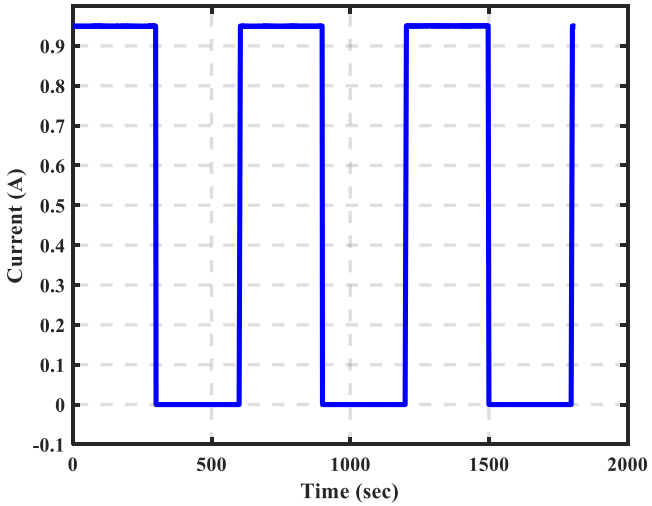

Figure 4.7: Pulse load discharge current at 0.95 A.

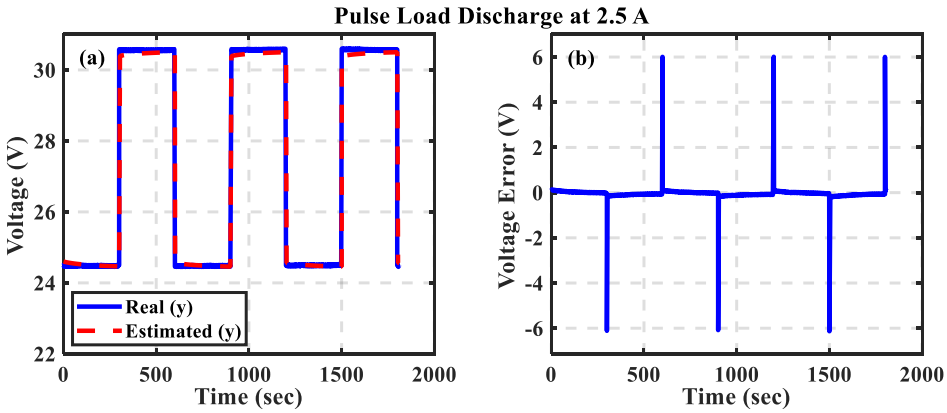

Figure 4.8: Pulse load discharge validation at 2.5 A with 75-mV average absolute voltage error in (a), and the voltage error vs. time in (b).

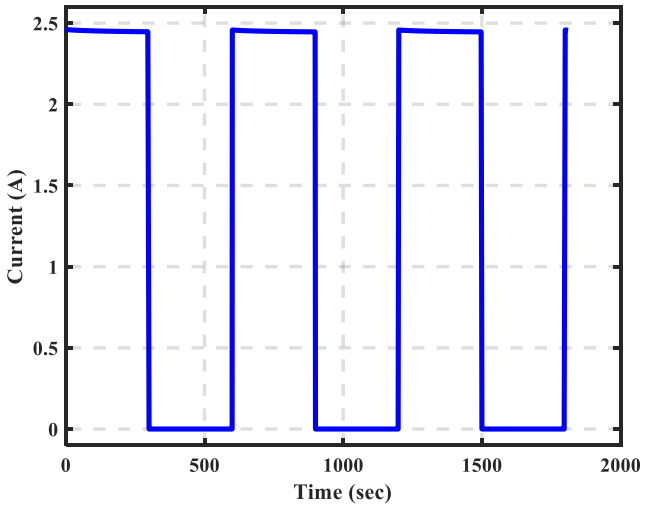

Figure 4.9: Pulse load discharge current at 2.5 A.

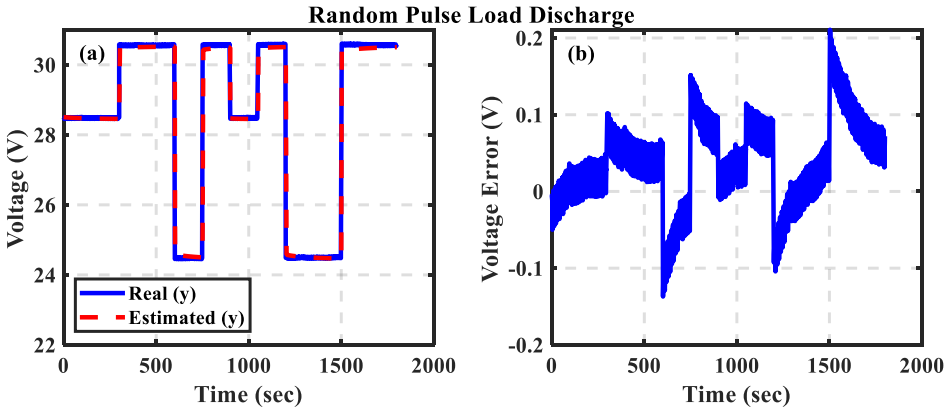

Figure 4.10: Pulse load discharge validation at variable loads with 60.9-mV average absolute voltage error in (a), and the voltage error vs. time in (b).

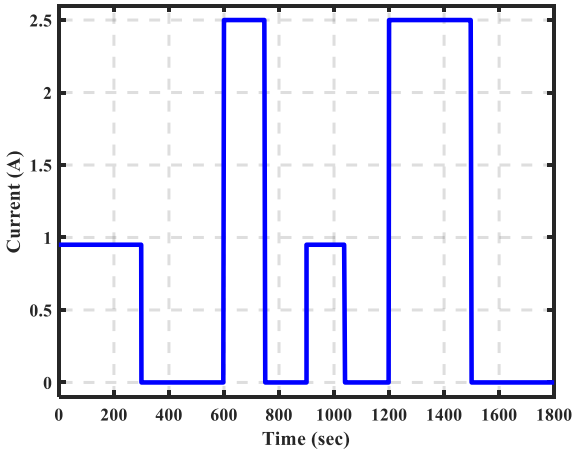

Figure 4.11: Random pulse loads discharge.

4.2. PEMFC Stack Size Effect

The proposed model and the parameters estimation methodology can be applied for any PEMFC stack size. In this section, 30-W PEMFC stack is used to validate the model and obtain the model parameters to compare it to the 200-W PEMFC stack. The data were collected from the experimental setup shown in Figure 3.10. Then, the three steps procedure in Figure 3.1 is carried out to estimate all the model parameters.

The first step is to obtain the open-circuit voltage parameters. The open-circuit voltage of the 30-W PEMFC stack and the hydrogen flow rate were measured at each 0.01 second until the Hydrostik is fully exhausted. Then, the parameters of equation (52) are obtained by curve fitting techniques and are given in Table 4.3. The real and the estimated open-circuit voltage for the 30-W PEMFC stack is shown in Figure 4.12

along with the estimation error vs. time. The average absolute voltage error is 26-mV only. The estimation error range is between -0.2 to 0.4 V.

Table 4.3: Open-circuit voltage relation parameters using Gaussian with 6 terms for 30-W PEMFC stack.

Parameter	$\hat{b}_1$	$\hat{b}_2$	$\hat{b}_3$	$\hat{b}_4$	$\hat{b}_5$	$\hat{b}_6$
Value	4.721	0.5592	0.05062	6.675	0.7799	0.1441
Parameter	$\hat{b}_7$	$\hat{b}_8$	$\hat{b}_9$	$\hat{b}_{10}$	$\hat{b}_{11}$	$\hat{b}_{12}$
Value	5.101	0.6725	0.1002	2.596	0.541	0.02556
Parameter	$\hat{b}_{13}$	$\hat{b}_{14}$	$\hat{b}_{15}$	$\hat{b}_{16}$	$\hat{b}_{17}$	$\hat{b}_{18}$
Value	11.41	1.019	0.2294	4.663	0.6072	0.07071

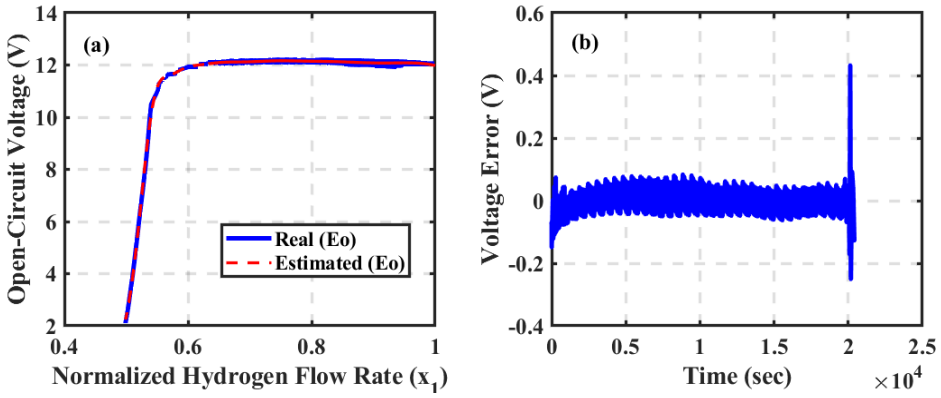

Figure 4.12: Real open-circuit voltage of the 30-W PEMFC stack vs. the estimated with 26-mV average absolute voltage error in (a), and the voltage error vs. time in (b).

In the second step, the APE technique has been applied to estimate the parameters of the two RC parallel combinations. Constant load discharge at 0.02 A is used to estimate the voltage dynamics parameters. The load is connected to the terminal of the 30-W PEMFC stack and the measurements are taken at every 0.01 seconds until the Hydrostik is fully exhausted. The parameters of the two RC parallel combinations are similar, as for the 200-W PEMFC as given in Table 3.11.

In the last step, the series resistance parameters are obtained that are given in Table 4.4. These parameters are different from the parameters for the 200-W PEMFC stack. Therefore, both open-circuit voltage and series resistance parameters are changing for different PEMFC stack sizes. While the parameters of the two RC parallel combinations are not affected by the stack size.

The real terminal voltage vs. the estimated terminal voltage is shown in Figure 4.13 at 0.02 A constant discharge current. The average absolute voltage error is 20.7-mV. The error between the estimated and real values is between -0.25 to 0.4 V. Thus, the model is valid and accurate for all PEMFC stack sizes. The current vs. time is shown in Figure 4.14.

Table 4.4: Estimated series resistance parameters at 0.02 A discharge current.

Parameter	$\hat{b}_{31}$	$\hat{b}_{32}$	$\hat{b}_{33}$
Value	0.001634	20.65	16.04

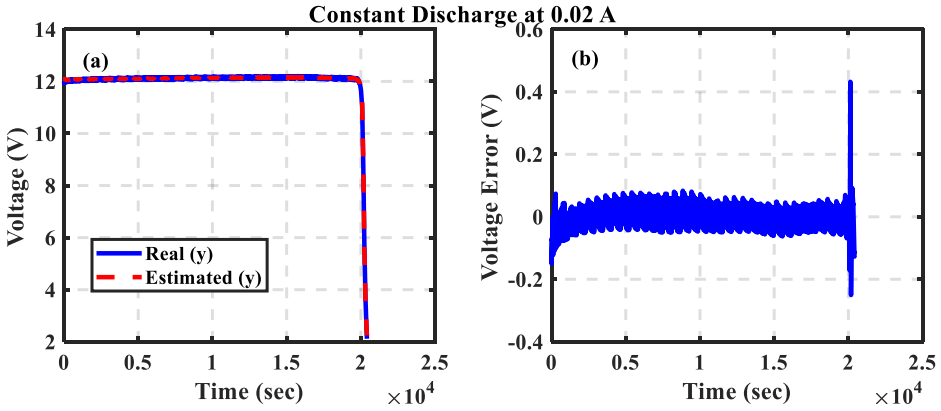

Figure 4.13: Real output voltage of the 30-W PEMFC stack vs. the estimated one with 20.7-mV average absolute voltage error at 0.02 A in (a), and the voltage error vs. time in (b).

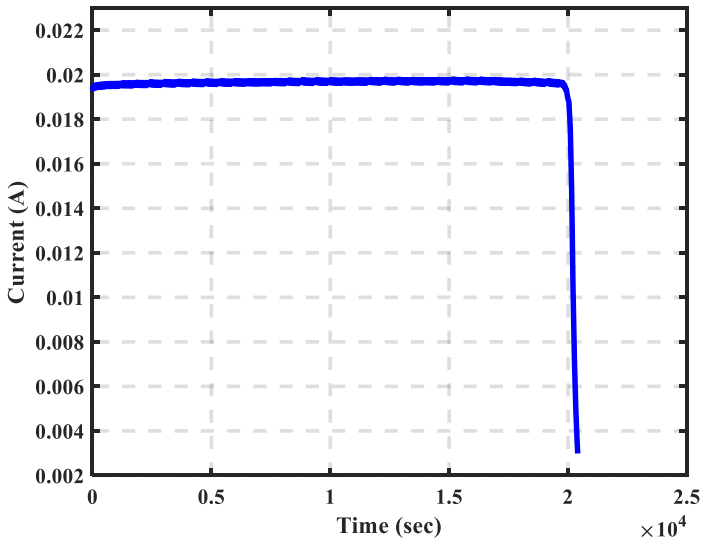

Figure 4.14: Constant discharge current at 0.02 A.

4.3. Error Statistics

The error statistics are evaluated by combining all the error vectors from all the conducted experiments. First, the histogram of the voltage estimation error is plotted in Figure 4.15. The y-axis represents the number of samples, and the x-axis represents the terminal voltage estimation error. This error is the difference between the real data from the experiments and the estimated data from the proposed model. It is illustrated that the estimation errors are between -0.2 to 0.2 V. Most of the data has absolute estimation error that is less than 0.1 V. In Figure 4.16, the cumulative distribution is shown of the terminal voltage estimation error. The x-axis shows the percentage error while the y-axis shows the percentage of the sample points. From this, it is obvious that approximately 95.84% of the samples lie between ± 0.1 percent error.

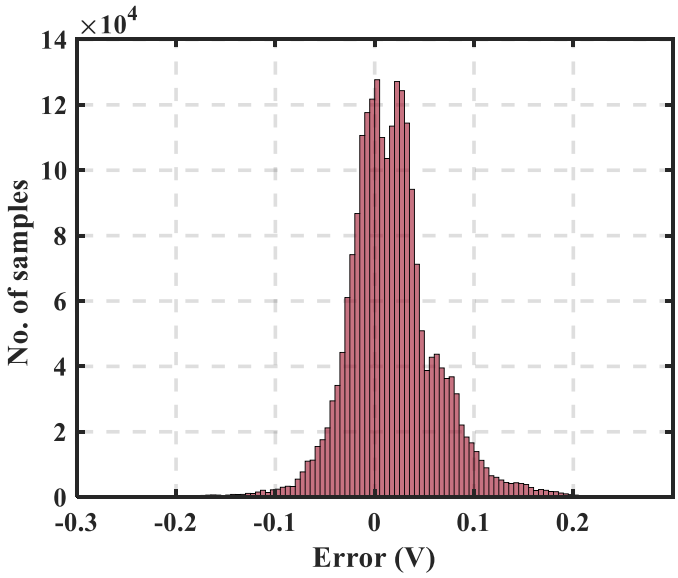

Figure 4.15: Voltage estimation error histogram.

The results in this chapter illustrate that the proposed model is novel, simple, accurate, and captures the essential electrical performance characteristics of a PEMFC stack. Also, it can be applied for different types and sizes of fuel cells. This model is valid for different load conditions and responds to any transients in the current. The model provides single-variable relations for the equivalent electrical circuit elements that make it simple and captures the nonlinear behavior of the PEMFC stack accurately. Also, using the UAS-based APE process to estimate all the model parameters help on reducing the experimental effort. Only five experiments are needed to extract the model parameters (four open-circuit tests and one constant load discharge test). The series

resistance value increases as the load current decreases as illustrated by the change of the series resistance values with the load current. For different fuel cell stack sizes, the parameters of the open-circuit voltage and series resistance are changing, while the parameters of the two RC parallel combinations are not. The error statistics results show the accuracy of the model prediction when compared to the real experimental data.

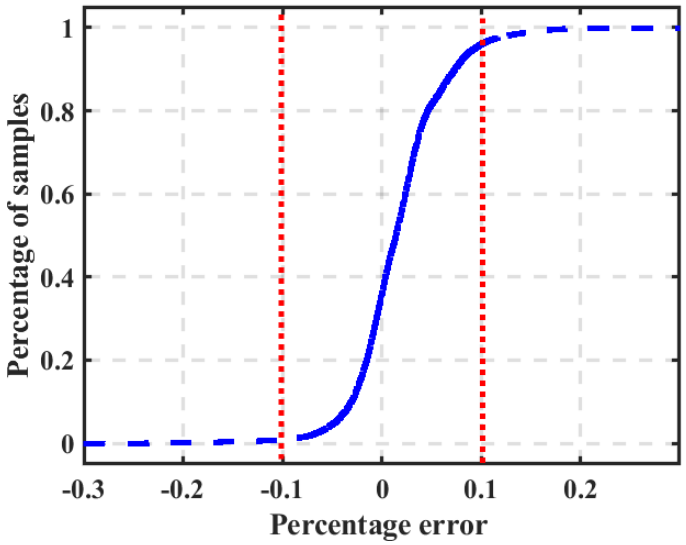

Figure 4.16: Cumulative distribution of percentage estimation error.

Chapter 5. Conclusion and Future Work

In conclusion, this work develops an equivalent electric circuit model for capturing runtime voltage-current (V-I) characteristics of a proton-exchange membrane fuel cell (PEMFC) stack. The model is based on the Chen and Mora (CM) battery model because battery and fuel cell share similar electrical characteristics. The electric circuit parameters of the model developed in this thesis, are functions of the normalized hydrogen flow rate, this is analogous to state of charge (SoC) used in several well-known battery models. Novel relationships are further developed for estimating the open-circuit voltage and series resistance characteristics. Additionally, the Universal Adaptive Stabilization (UAS) based adaptive parameters estimation (APE) strategy is used with the above-mentioned model, for the first time as per the author's knowledge, for model parameters estimation. The application of UAS-based APE for parameters estimation of a PEMFC stack reduces the experimental effort. Five experiments are required to estimate the model parameters in this work, these are four experiments to estimate the open-circuit voltage parameters and one constant discharge load test to estimate the terminal voltage dynamics parameters. Usually many more tests are required to estimate model parameters of a similar complex model for a PEMFC stack.

The model developed in this thesis is tested at different load conditions that are constant load discharge and pulsed load discharge for the 200-W PEMFC stack. The results show low average absolute voltage error in the order of millivolts for all the tests. Also, the stack size effect is studied by comparing the parameters of the 200-W PEMFC stack to the 30-W PEMFC stack. It is observed that the parameters of the open-circuit voltage and series resistance depend on the PEMFC stack size, other model parameters are not affected. The error statistics presented show the accuracy of the proposed model, and the UAS-based methodology, for model parameters estimation. The estimation error between the measured terminal voltage and the estimated terminal voltage lies between -0.2 to 0.2 V only. Also, 95.84% of the all samples of estimated terminal voltage have between ± 0.1 percent error compared to the actual terminal voltage.

The model developed in this thesis and the corresponding UAS-based strategy can be applied to estimate model parameters of other types of fuel cells in future.

References

[1] EG&G Technical Services, Inc., *Fuel Cell Handbook*, Seventh. Morgantwon, West Virginia: U.S. Department of Energy Office of Fossil Energy National Energy Technology Laboratory, 2004.

[2] M. Chen and G. A. Rincon-Mora, "A Compact Electrical Model for Microscale Fuel Cells Capable of Predicting Runtime and I-V Polarization Performance," *IEEE Trans. Energy Convers.*, vol. 23, no. 3, pp. 842–850, Sep. 2008.

[3] J. Larminie and A. Dicks, *Fuel cell systems explained*, 2nd ed. Chichester, West Sussex: J. Wiley, 2003.

[4] F. Barbir, "PEM electrolysis for production of hydrogen from renewable energy sources," *Sol. Energy*, vol. 78, no. 5, pp. 661–669, May 2005.

[5] C. Wang, M. H. Nehrir, and S. R. Shaw, "Dynamic models and model validation for PEM fuel cells using electrical circuits," *IEEE Trans. Energy Convers.*, vol. 20, no. 2, pp. 442–451, Jun. 2005.

[6] P. Pei, M. Ouyang, W. Feng, L. Lu, H. Huang, and J. Zhang, "Hydrogen pressure drop characteristics in a fuel cell stack," *Int. J. Hydrog. Energy*, vol. 31, no. 3, pp. 371–377, Mar. 2006.

[7] M. W. Fowler, R. F. Mann, J. C. Amphlett, B. A. Peppley, and P. R. Roberge, "Incorporation of voltage degradation into a generalised steady state electrochemical model for a PEM fuel cell," *J. Power Sources*, vol. 106, no. 1, pp. 274–283, Apr. 2002.

[8] T. E. Springer, T. A. Zawodzinski, and S. Gottesfeld, "Polymer Electrolyte Fuel Cell Model," *J. Electrochem. Soc.*, vol. 138, no. 8, pp. 2334–2342, Aug. 1991.

[9] R. F. Mann, J. C. Amphlett, M. A. I. Hooper, H. M. Jensen, B. A. Peppley, and P. R. Roberge, "Development and application of a generalised steady-state electrochemical model for a PEM fuel cell," *J. Power Sources*, vol. 86, no. 1, pp. 173–180, Mar. 2000.

[10] R. M. Rao, D. Bhattacharyya, R. Rengaswamy, and S. R. Choudhury, "A two-dimensional steady state model including the effect of liquid water for a PEM fuel cell cathode," *J. Power Sources*, vol. 173, no. 1, pp. 375–393, Nov. 2007.

[11] Q. Guo and R. E. White, "A Steady-State Impedance Model for a PEMFC Cathode," *J. Electrochem. Soc.*, vol. 151, no. 4, pp. E133–E149, Apr. 2004.

[12] S.-H. Ge and B.-L. Yi, “A mathematical model for PEMFC in different flow modes,” *J. Power Sources*, vol. 124, no. 1, pp. 1–11, Oct. 2003.

[13] J. M. Correa, F. A. Farret, L. N. Canha, and M. G. Simoes, “An Electrochemical-Based Fuel-Cell Model Suitable for Electrical Engineering Automation Approach,” *IEEE Trans. Ind. Electron.*, vol. 51, no. 5, pp. 1103–1112, Oct. 2004.

[14] W. Choi, P. N. Enjeti, and J. W. Howze, “Development of an equivalent circuit model of a fuel cell to evaluate the effects of inverter ripple current,” in *Nineteenth Annual IEEE Applied Power Electronics Conference and Exposition, 2004. APEC ’04*, Anaheim, CA, USA, 2004, vol. 1, pp. 355-361

[15] A. A. Kulikovsky, “Hydrogen crossover impedance of a PEM fuel cell at open circuit,” *Electrochimica Acta*, vol. 247, pp. 730–735, Sep. 2017.

[16] R. Jiang and D. Chu, “Voltage–time behavior of a polymer electrolyte membrane fuel cell stack at constant current discharge,” *J. Power Sources*, vol. 92, no. 1, pp. 193–198, Jan. 2001.

[17] J. T. Pukrusphan, *Modeling and Control of Fuel Cell Systems and Fuel Processors*. Dissertation (Ph.D.)-University of Michigan, Ann Arbor, Michigan, USA, 2003.

[18] R. M. Darling and J. P. Meyers, “Kinetic Model of Platinum Dissolution in PEMFCs,” *J. Electrochem. Soc.*, vol. 150, no. 11, pp. A1523–A1527, Nov. 2003.

[19] S. Yerramalla, A. Davari, A. Feliachi, and T. Biswas, “Modeling and simulation of the dynamic behavior of a polymer electrolyte membrane fuel cell,” *J. Power Sources*, vol. 124, no. 1, pp. 104–113, Oct. 2003.

[20] C. Kunusch, P. F. Puleston, M. A. Mayosky, and A. P. Husar, “Control-Oriented Modeling and Experimental Validation of a PEMFC Generation System,” *IEEE Trans. Energy Convers.*, vol. 26, no. 3, pp. 851–861, Sep. 2011.

[21] J. D. Rojas, C. Kunusch, C. Ocampo-Martinez, and V. Puig, “Control-Oriented Thermal Modeling Methodology for Water-Cooled PEM Fuel-Cell-Based Systems,” *IEEE Trans. Ind. Electron.*, vol. 62, no. 8, pp. 5146–5154, Aug. 2015.

[22] J. Ishaku, N. Lotfi, H. Zomorodi, and R. G. Landers, “Control-oriented modeling for open-cathode fuel cell systems,” in *2014 American Control Conference*, Portland, OR, USA, 2014, pp. 268–273.

[23] J. A. Salva, A. Iranzo, F. Rosa, E. Tapia, E. Lopez, and F. Isorna, “Optimization of a PEM fuel cell operating conditions: Obtaining the maximum performance

polarization curve," *Int. J. Hydrog. Energy*, vol. 41, no. 43, pp. 19713–19723, Nov. 2016.

[24] D. Yu and S. Yuvarajan, "Electronic circuit model for proton exchange membrane fuel cells," *J. Power Sources*, vol. 142, no. 1, pp. 238–242, Mar. 2005.

[25] A. Hernandez, D. Hissel, and R. Outbib, "Modeling and Fault Diagnosis of a Polymer Electrolyte Fuel Cell Using Electrical Equivalent Analysis," *IEEE Trans. Energy Convers.*, vol. 25, no. 1, pp. 148–160, Mar. 2010.

[26] M. J. Khan and M. T. Iqbal, "Dynamic modeling and simulation of a small wind–fuel cell hybrid energy system," *Renew. Energy*, vol. 30, no. 3, pp. 421–439, Mar. 2005.

[27] T. Douglas, "Dynamic modelling and simulation of a solar-PV hybrid battery and hydrogen energy storage system," *J. Energy Storage*, vol. 7, pp. 104–114, Aug. 2016.

[28] M. Uzunoglu and M. S. Alam, "Dynamic modeling, design and simulation of a PEM fuel cell/ultra-capacitor hybrid system for vehicular applications," *Energy Convers. Manag.*, vol. 48, no. 5, pp. 1544–1553, May 2007.

[29] M. Uzunoglu, O. C. Onar, and M. S. Alam, "Modeling, control and simulation of a PV/FC/UC based hybrid power generation system for stand-alone applications," *Renew. Energy*, vol. 34, no. 3, pp. 509–520, Mar. 2009.

[30] O. C. Onar, M. Uzunoglu, and M. S. Alam, "Dynamic modeling, design and simulation of a wind/fuel cell/ultra-capacitor-based hybrid power generation system," *J. Power Sources*, vol. 161, no. 1, pp. 707–722, Oct. 2006.

[31] A. Forrai, H. Funato, Y. Yanagita, and Y. Kato, "Fuel-Cell Parameter Estimation and Diagnostics," *IEEE Trans. Energy Convers.*, vol. 20, no. 3, pp. 668–675, Sep. 2005.

[32] A. Askarzadeh and L. dos S. Coelho, "A backtracking search algorithm combined with Burger's chaotic map for parameter estimation of PEMFC electrochemical model," *Int. J. Hydrog. Energy*, vol. 39, no. 21, pp. 11165–11174, Jul. 2014.

[33] M. Chen, S. Member, G. A. Rincón-mora, and S. Member, "Accurate Electrical Battery Model Capable of Predicting Runtime and I-V Performance," *IEEE Trans. Energy Convers.*, pp. 504–511, 2006.

[34] D. Ali, S. Mukhopadhyay, H. Rehman, and A. Khurram, “UAS based Li-ion battery model parameters estimation,” *Control Eng. Pract.*, vol. 66, pp. 126–145, Sep. 2017.

[35] “References | Engaged in Thermodynamics.” [Online]. Available: http://cset.mnsu.edu/engagethermo/appendices_04.html. [Accessed: 23-Apr-2019].

[36] J. L. Silveira, Ed., *Sustainable Hydrogen Production Processes*. Cham: Springer International Publishing, 2017.

[37] J. Kim, S.-M. Lee, S. Srinivasan, and C. E. Chamberlin, “Modeling of Proton Exchange Membrane Fuel Cell Performance with an Empirical Equation,” *J. Electrochem. Soc.*, vol. 142, no. 8, pp. 2670–2674, Aug. 1995.

[38] F. Laurencelle *et al.*, “Characterization of a Ballard MK5-E Proton Exchange Membrane Fuel Cell Stack,” *Fuel Cells*, vol. 1, no. 1, pp. 66–71, May 2001.

[39] Y. Li and Y. Chen, “When is a Mittag–Leffler function a Nussbaum function?,” *Automatica*, vol. 45, no. 8, pp. 1957–1959, Aug. 2009.

[40] S. Mukhopadhyay and F. Zhang, “A high-gain adaptive observer for detecting Li-ion battery terminal voltage collapse,” *Automatica*, vol. 50, no. 3, pp. 896–902, Mar. 2014.

[41] S. Mukhopadhyay, Y. Li, and Y. Chen, “Experimental Studies of a Fractional Order Universal Adaptive Stabilizer,” in *2008 IEEE/ASME International Conference on Mechtronic and Embedded Systems and Applications*, 2008, pp. 591–596.

[42] “Mittag-Leffler function, M-file, cmex DLL, and S-function - File Exchange - MATLAB Central.” [Online]. Available: https://ch.mathworks.com/matlabcentral/fileexchange/20731. [Accessed: 06-Aug-2018].

[43] M. Petzl and M. A. Danzer, “Advancements in OCV Measurement and Analysis for Lithium-Ion Batteries,” *IEEE Trans. Energy Convers.*, vol. 28, no. 3, pp. 675–681, Sep. 2013.

[44] “Aerostak.” [Online]. Available: https://www.hes.sg/aerostak. [Accessed: 27-Mar-2019].

[45] “Horizon Fuel Cell Technologies,” *Horizon Fuel Cell Technologies*. [Online]. Available: https://www.horizonfuelcell.com. [Accessed: 18-Aug-2018].

[46] “Hydrofill Pro.” [Online]. Available: http://www.fuelcellstore.com/horizon-hydrofill-pro-fch-020. [Accessed: 18-Aug-2018].

[47] “Hydrostik Pro.” [Online]. Available: https://www.fuelcellstore.com/hydrogen-equipment/horizon-hydrostik-pro-fch-020. [Accessed: 27-Apr-2019].

[48] “Xi’an Yunyi Instrument Co., Ltd.” [Online]. Available: http://www.yunyi-instrument.com/. [Accessed: 18-Aug-2018].

[49] “Siargo Ltd.” [Online]. Available: http://www.siargo.us/. [Accessed: 18-Aug-2018].

[50] W. J. Buttner, M. B. Post, R. Burgess, and C. Rivkin, “An overview of hydrogen safety sensors and requirements,” *Int. J. Hydrog. Energy*, vol. 36, no. 3, pp. 2462–2470, Feb. 2011.

[51] “Hydrogen Detection System | Hydrogen Gas Monitor and Detector,” *NTM Sensors*.

[52] “HES energy systems | powering an autonomous world,” *hes energy systems | powering an autonomous world*. [Online]. Available: https://www.hes.sg. [Accessed: 19-Oct-2018].

[53] “Horizon 30W PEM Fuel Cell.” [Online]. Available: http://www.fuelcellstore.com/fuel-cell-stacks/horizon-h30-fuel-cell. [Accessed: 19-Aug-2018].

Vita

Aya Mohamad Taieb received her primary and secondary education in Umm Al-Quwain, UAE. She received her B.Sc. degree in Sustainable and Renewable Energy Engineering from the University of Sharjah in 2017.

In September 2017, she joined the Electrical Engineering master's program in the American University of Sharjah as a graduate teaching assistant. During her master's study, she co-authored two papers which were presented in international conferences. Her research interests are in the area of fuel cells modelling, energy storage systems and transmission, and third-generation solar cells.